automation

MDPI

Article

Substrate-Driven PLC Control (SD-PLC) Design for Fixed-Dome Biodigesters: A Rheology- and Energy-Constrained Methodology with a Guinea Pig Manure Co-Digestion Case Study

Yoisdel Castillo Alvarez [1,*], Anibal Salvador Wenceslao Ferro Diaz [1], Deyvi Gair Baltazar Cari [1], Reinier Jiménez Borges [2,*], Carlos Diego Patiño Vidal [1], Fanny Mabel Carhuancho León [3], Romel Ángel Cárdenas Javier [1] and Roberto Pfuyo Muñoz [4]

1 Department of Mechanical Engineering, Universidad Tecnológica del Perú, Lima 15046, Peru
2 Department of Mechanical Engineering, Faculty of Engineering, Universidad de Cienfuegos "Carlos Rafael Rodríguez", Cienfuegos 59430, Cuba
3 Department of Environmental Engineering, Universidad Nacional Agraria La Molina (UNALM), Lima 15024, Peru
4 Department of Mechanical Engineering, Universidad Nacional Tecnológica de Lima Sur (UNTELS), Lima 15842, Peru
* Correspondence: c19773@utp.edu.pe (Y.C.A.); rjimenezborges@gmail.com (R.J.B.)

Abstract

The automation of biodigesters using programmable logic controllers (PLCs) is well established, yet mixing schedules are configured empirically, regardless of substrate characteristics. This study proposes a Substrate-Driven PLC Control (SD-PLC) methodology for fixed-dome biodigesters, in which every timing setpoint is derived from a measured substrate property: the homogenization pulse from the rheological mixing time (Metzner–Otto regime), the maintenance interval from a stratification and a substrate–biomass contact criterion, the duty-cycle ceiling from a net energy balance, and a safety gate from acid–base behavior (pH/EC). The methodology is instantiated on a 13.86 m^3 fixed-dome biodigester in the Chillón Valley (Lima, Peru), co-digesting organic waste and guinea pig manure (30:70; theoretical methane potential 371 mL CH_4 g^{-1} VS; field conversion ≈ 21%). The impeller operates in the transitional regime ($Re \approx 0.9–2.6 \times 10^3$), the homogenization pulse is ≈22 min, and the reconciled duty cycle ($\delta \approx 0.13$) remains a factor of four below the energy ceiling ($\delta^* \approx 0.56$). An influence × feasibility matrix identifies a low-cost sensor set (pH, electrical conductivity, temperature, level) that gates mixing. A reduced COD-based dynamic model shows that, under acid shock, continuous mixing suppresses methanogenesis through shear while the absence of mixing fails through contact deficit, so that only the stability-first strategy preserves the process. The principal contribution is the methodology itself—a reproducible mapping from substrate characterization to PLC timing design—rather than the hardware.

Keywords: substrate-driven PLC control; fixed-dome biodigester; slurry rheology; mixing duty cycle; guinea pig excreta co-digestion

Check for updates

Academic Editor: Chenliang Liu

Received: 8 July 2026
Revised: 3 August 2026
Accepted: 10 August 2026
Published: 31 August 2026

Copyright: © 2026 by the authors. Licensee MDPI, Basel, Switzerland. This article is an open access article distributed under the terms and conditions of the Creative Commons Attribution (CC BY) license.

1. Introduction

The inadequate management of agricultural and livestock organic waste remains a persistent structural challenge in rural areas, where manure, crop residues, and the household organic fraction are frequently accumulated or disposed of without adequate treatment [1,2]. Livestock production accounts for approximately 7.1 Gt CO_2-eq of global

greenhouse gas emissions annually, representing nearly 14.5% of total anthropogenic emissions, with methane and nitrous oxide released from manure management as the principal contributors [3]. In this context, anaerobic digestion (AD) provides a circular-economy pathway that converts organic waste into biogas and biofertilizer while simultaneously mitigating environmental pollution and reducing dependence on fossil fuels [4]. Co-digestion studies consistently show that combining manure with complementary substrates enhances methane yield compared with mono-digestion by improving the carbon-to-nitrogen (C/N) ratio and promoting a more diverse microbial community [4–6].

Nevertheless, the mere availability of the technology does not guarantee its successful implementation. Recent reviews of small-scale biodigesters in developing countries indicate that their performance depends critically on design quality, substrate suitability, and proper maintenance, while technical barriers—including the lack of standardized designs, insufficient technical support, and inadequate operation—continue to hinder their widespread adoption and long-term reliability [1,2]. A substantial proportion of household biodigesters in developing countries is estimated to experience operational failures attributable to poor design decisions and inappropriate substrate management [1,7]. Consequently, the challenge extends beyond simply deploying biodigesters; it lies in developing systems that are both technically robust and operationally reliable.

Among the most widely adopted low-cost configurations, the fixed-dome (Chinese-type) biodigester occupies a prominent position because of its structural simplicity, low construction cost, and long service life [1,2]. However, its limitations become evident when the reactor hydrodynamics are examined. Conventional Chinese fixed-dome digesters typically operate with long hydraulic retention times and low influent solids concentrations owing to insufficient mixing. To mitigate this limitation, Jegede et al. [8] developed an optimized pilot-scale (500 L) Chinese fixed-dome biodigester incorporating a self-agitating mechanism, while a subsequent computational fluid dynamics (CFD) analysis showed that the addition of baffles improves hydraulic performance and reduces the fraction of semi-dead zones through pressure-driven self-mixing cycles [9,10]. More recently, CFD analyses of Chinese fixed-dome biodigesters have confirmed that scum formation, dead zones, and inadequate mixing remain critical operational challenges, and that optimizing the mixing frequency enhances methane production by disrupting the scum layer and improving substrate distribution [11,12]. These studies provide compelling evidence that the hydrodynamic behavior of the Chinese fixed-dome biodigester remains an unresolved engineering problem, a conclusion consistent with the broader CFD literature on anaerobic digesters [13]. However, the proposed solutions have focused primarily on geometric modifications or self-induced mixing mechanisms rather than on programmable, actively controlled mixing strategies.

Mixing is one of the most critical yet frequently underestimated variables in AD. Comprehensive reviews have shown that mixing directly influences sludge homogeneity, dead-zone reduction, scum prevention, and power consumption, while impeller geometry significantly affects overall mixing efficiency [14,15]. More importantly, mixing performance should be evaluated in terms of net energy efficiency. Kariyama et al. [16] concluded that there is no energetic justification for operating continuously stirred tank digesters under continuous mixing when energy efficiency is the primary objective, and that optimally designed intermittent mixing outperforms continuous operation. This is not a marginal effect: at full scale, mixing may account for approximately one-third to one-half of a biogas plant's electricity consumption [17]. Consequently, both mixing intensity and duty cycle are decisive factors in determining whether a small-scale AD system achieves a positive net energy balance. Recent process-optimization reviews reaffirm this conclusion [18,19]. The current body of evidence therefore no longer supports the simplistic assumption that

"more mixing is better"; instead, it supports optimized mixing tailored to the characteristics of both the substrate and the reactor.

A prerequisite for defining such an optimum is the rheological characterization of the substrate, an aspect that is rarely addressed explicitly in the fixed-dome biodigester literature. Manure slurries are non-Newtonian fluids that exhibit pseudoplastic (shear-thinning) behavior, with apparent viscosity decreasing as the shear rate increases. Their rheology is adequately described by the power-law model at relatively low solids concentrations and by the Herschel–Bulkley model, which incorporates yield stress, at higher solids contents [20,21]. This has two important implications that are commonly overlooked in fixed-dome biodigester design. First, the impeller Reynolds number cannot be calculated using a constant viscosity. Instead, the apparent viscosity at the impeller shear rate must be estimated, conventionally through the Metzner–Otto concept [22], which determines whether the flow regime is laminar, transitional, or turbulent and therefore which power correlation is applicable [23]. Second, because both apparent viscosity and yield stress govern sedimentation, stratification, and scum formation, they ultimately determine the mechanical mixing requirements and, consequently, the parasitic energy demand associated with mixing.

In parallel with these developments, automation has become increasingly important in AD systems. PLC-based digesters integrated with SCADA architectures for the management of mixing, liquid levels, and operational safety have become common industrial practice, and comprehensive reviews have summarized the current state of instrumentation and process control for anaerobic digesters [24,25], a picture confirmed by the most recent surveys of the field [26]. However—and this constitutes the central motivation of the present study—the reported implementations configure mixing timers empirically, according to manufacturer default settings or generic operational recommendations. None derive mixing time setpoints directly from the measured properties of the processed substrate. This distinction is crucial because the mixing demand—how much homogenization is required, how frequently settled solids should be resuspended, how much energy mixing consumes, and under which biological conditions mixing becomes detrimental—is governed by substrate rheology, sedimentation behavior, energy performance, and acid–base dynamics. A control law calibrated for one substrate cannot be assumed to be transferable to another, whereas a control law calibrated for none is fundamentally arbitrary.

The Andean context further reinforces this need. In Peru, rural livestock production includes the guinea pig (Cavia porcellus) as a culturally and economically important species, while a large proportion of the rural Andean population still lacks access to clean cooking fuels [27,28]. Anaerobic digestion of manure under low-temperature (psychrophilic to low-mesophilic, 16–25 °C) conditions has been extensively investigated in low-cost tubular biodigesters across the Peruvian and Bolivian Andes, where methane yields are primarily constrained by temperature [27–30]. Likewise, the co-digestion of guinea pig manure with Andean lignocellulosic residues has demonstrated promising mesophilic performance [31], Co-digestion of guinea pig manure with cow manure has likewise been assessed in Peruvian tubular digesters [32], and lignocellulosic co-substrates have been evaluated with South American camelid manure [33]. While techno-economic and multi-criteria assessments have confirmed the suitability of these technologies for rural Peru [2,28]. Nevertheless, none of these studies addresses the design of mixing control as a function of substrate properties.

This study fills that gap by proposing a Substrate-Driven PLC Control (SD-PLC) methodology for fixed-dome biodigesters. The proposed framework is a reproducible procedure that maps measured substrate characteristics into PLC timing setpoints, such that the homogenization pulse duration, maintenance interval, duty-cycle upper bound, and biological safety gate emerge as calculated outputs rather than empirical assumptions.

The methodology is instantiated and bounded through a case study of an existing 13.86 m^3 fixed-dome biodigester located in the Chillón Valley (Lima, Peru), co-digesting organic waste and guinea pig manure. This case study is intentionally presented as a demonstration of the methodology and is explicitly distinguished from the authors' previous work on the same reactor, which focused on geometric and operational design improvements [7] and on reactive pH/EC control [34], but did not propose a substrate-driven control design procedure. Accordingly, the contribution claimed in this work is the methodology itself, rather than the biodigester or its hardware implementation.

The novelty of this work is therefore not the hardware, the substrate, or the ladder logic—all of which are conventional—but the derivation chain that links them. Four timing decisions habitually taken by default are here converted into calculated outputs: (i) the homogenization pulse $t_{on,h}$ is obtained from the Metzner–Otto apparent viscosity and the impeller pumping capacity rather than from a factory timer; (ii) the maintenance interval $t_{off,m}$ is bounded simultaneously by a sedimentation criterion in a yield-stress medium and by a substrate–biomass contact criterion, which promotes the yield stress τ_0 from an unmeasured property to a design input; (iii) the duty cycle δ is capped by an explicit net-energy ceiling δ^*, converting mixing from an operational habit into an energy-constrained decision variable; and (iv) the pH/EC gate subordinates the entire timing program to the acid–base state, inhibiting agitation precisely when shear is most damaging.

2. Materials and Methods

2.1. Study Area: Chillón Valley

The Chillón Valley, located north of Lima, Peru, is one of the principal agricultural and livestock production areas within the metropolitan region. Formed by the Chillón River basin, it combines crop cultivation, small-scale livestock farming, and expanding urban development along an altitudinal gradient extending from the arid coastal plain to the Andean foothills. Intensive guinea pig farming is a common household activity, and the resulting manure, together with the organic fraction of domestic and agricultural waste, represents an abundant feedstock for local energy recovery. The biodigester investigated in this study (Figure 1) is located within this valley (approximately 11.87° S, 77.06° W) and operates under ambient conditions without external heating, within the low-mesophilic temperature range characteristic of the region. It consists of a buried fixed-dome masonry structure (brick and reinforced concrete) equipped with inlet and outlet chambers, representative of the low-cost rural biodigesters widely deployed in the area.

2.2. Reference Reactor and Hydraulic Design

The total volume of the rectangular reactor (length l, width a, and height h) is given by Equation (1):

$$V = l \times a \times h. \tag{1}$$

The reactor is operated under semi-continuous feeding with a daily mass M of the co-digestion mixture (organic waste:guinea pig manure) diluted with water. Because the organic waste fraction possesses a high intrinsic moisture content, it contributes part of the required dilution water. Assuming a mixture density ρ, the daily volumetric flow rate is, as shown in Equation (2),

$$Q = \frac{M + M_w}{\rho}, \tag{2}$$

where M_w is the mass of added water. For a target hydraulic retention time (HRT), the required digestion volume and the construction volume (including a gas-dome overdesign factor f_{sv}) are shown in Equation (3):

$$V_d = Q \cdot \mathrm{HRT}, \qquad V_{cd} = f_{sv}\, V_d. \tag{3}$$



Figure 1. Fixed-dome (Chinese-type) masonry biodigester investigated in the Chillón Valley (Lima, Peru). (**a**) Access hatch, steel cover and inlet chamber; (**b**,**c**) vertical shafts with stainless-steel marine propellers driven by geared motors; (**d**) buried masonry structure and control enclosure. The buried construction and the surrounding arid environment are representative of low-cost rural biodigester installations in the region.

The design criterion requires, as shown in Equation (4),

$$V \geq V_{cd}, \tag{4}$$

whose verification for the existing reactor is presented in the Section 3 using the measured input data. Throughout this work V denotes the constructed volume of Equation (1), whereas V_L denotes the mixed liquid working volume used in the mixing and dynamic calculations.

2.3. Characterization of the Substrate and Estimation of the Theoretical Methane Potential

Both co-substrates were characterized through proximate analysis (moisture content, W, and volatile matter, VM) and ultimate analysis (C, H, N, O, and S). The theoretical biochemical methane potential (BMP_{th}) was determined from the ultimate analysis using the Buswell–Boyle stoichiometric relationship [35–37]. For an empirical substrate formula $\mathrm{C}_a\mathrm{H}_b\mathrm{O}_c\mathrm{N}_d\mathrm{S}_e$ (whose stoichiometric coefficients are obtained from the elemental mass fractions), the reaction is expressed as Equation (5):

$$\mathrm{C}_a\mathrm{H}_b\mathrm{O}_c\mathrm{N}_d\mathrm{S}_e + w\,\mathrm{H_2O} \rightarrow n_{\mathrm{CH_4}}\,\mathrm{CH_4} + n_{\mathrm{CO_2}}\,\mathrm{CO_2} + d\,\mathrm{NH_3} + e\,\mathrm{H_2S}, \tag{5}$$

where

$$n_{\mathrm{CH_4}} = \frac{a}{2} + \frac{b}{8} - \frac{c}{4} - \frac{3d}{8} - \frac{e}{4},$$

and the theoretical methane yield per unit of volatile solids is shown in Equation (6):

$$\mathrm{BMP}_{th} = \frac{22.414\left(\frac{a}{2} + \frac{b}{8} - \frac{c}{4} - \frac{3d}{8} - \frac{e}{4}\right)}{12a + b + 16c + 14d + 32e} \times 10^3 \quad [\mathrm{mL\,CH_4\,g^{-1}\,VS}]. \tag{6}$$

For a co-digestion mixture, BMP_{th} is calculated as the volatile-solids-weighted average of the individual substrates, whereas the theoretical methane potential per unit fresh mass is obtained by multiplying BMP_{th} by the volatile matter fraction on a wet basis. The C/N ratio of the mixtures, by contrast, is computed on a dry-matter basis, following the convention of the anaerobic digestion literature; the two weighting bases are therefore not interchangeable. Theoretical BMP represents the upper limit attainable under complete substrate conversion and must therefore be distinguished from the experimentally measured methane potential. Their ratio defines the biodegradability index:

$$\mathrm{BDI} = \frac{\mathrm{BMP}_{exp}}{\mathrm{BMP}_{th}},$$

as proposed by Angelidaki et al. [37]. For the field-scale reactor, the realized methane production is expressed as BMP_{th} multiplied by a realization factor η_{bio}, which serves as an operational surrogate for the biodegradability index under the ambient low-mesophilic operating conditions of the reactor. Consequently, the proposed mixing strategy is formulated quantitatively as an increase in η_{bio}.

2.4. Substrate Rheological Characterization

The density of each mixture was determined as $\rho = m/v$. The co-digestion slurry was treated as a pseudoplastic non-Newtonian fluid, whose shear stress–shear rate relationship was described using the Ostwald–de Waele (power-law) model, with the Herschel–Bulkley extension adopted when yield stress is present [20,21], shown in Equation (7):

$$\tau = K\dot{\gamma}^n, \qquad \tau = \tau_0 + K\dot{\gamma}^n, \tag{7}$$

where τ is the shear stress, $\dot{\gamma}$ is the shear rate, K is the consistency index, n is the flow behavior index ($n < 1$ for shear-thinning fluids), and τ_0 is the yield stress. The yield stress of agricultural digestate scales exponentially with total solids content and depends strongly on particle size [38], and its measurement in coarse, fibrous biomass requires dedicated devices and sampling protocols rather than standard rotational geometries [39,40]. Representative density and apparent-viscosity values were compiled for guinea pig manure and for three manure-to-water dilution ratios (1:2, 1:2.5, and 1:3) to bound the expected operating range. Because the organic waste fraction exhibits a high moisture content ($W = 87.9\%$), it acts simultaneously as a co-substrate and as a natural diluent. The flow-curve parameters (K, n, τ_0) of the actual slurry have not been determined, so the apparent viscosity is reported as a representative range rather than as a calibrated model; the consequences are treated in Section 4.4.

2.5. Mixing Regime: Metzner–Otto Apparent Viscosity and Impeller Reynolds Number

Because the apparent viscosity of a pseudoplastic slurry depends on the local shear rate, the impeller Reynolds number cannot be calculated using a constant viscosity. The Metzner–Otto concept [22] relates the average shear rate in the impeller region to the rotational speed according to

$$\dot{\gamma}_{avg} = k_{MO}\, N,$$

where $k_{MO} \approx 10$–12 for marine propellers and turbine impellers. The apparent viscosity is then evaluated at $\dot{\gamma}_{avg}$ using the power-law model,

$$\mu_{app} = K\dot{\gamma}_{avg}^{n-1},$$

and the impeller Reynolds number is calculated as Equation (8):

$$Re = \frac{\rho N D^2}{\mu_{app}}, \tag{8}$$

where D is the impeller diameter. The flow regime is classified as laminar ($Re < 10$), transitional ($10 < Re < 10^4$), or turbulent ($Re > 10^4$), and the corresponding power correlation is selected accordingly.

This route is prescribed but not numerically closed here: since K and n have not been measured, the apparent viscosity used in the Results rather than computed from the flow curve.

2.6. Impeller Power and Installed Mixing Configuration

The shaft power required by the marine propeller is estimated from

$$P = N_p \rho N^3 D^5,$$

where N_p is the power number. It should be emphasized that this relationship is valid only when an appropriate value of N_p is employed for the corresponding flow regime: approximately constant under turbulent conditions, but increasing as Re decreases within the transitional and laminar regimes, approaching $N_p = K_p/Re$ in the laminar limit. Since the calculated operating condition falls within the transitional regime (Section 2.5), the use of a turbulent-flow power number provides only an upper estimate of the hydraulic power requirement. In practice, the installed motor power is additionally governed by start-up torque requirements, scum and settled-solids resuspension, and an appropriate service factor; CFD studies of high-solids digestion confirm that mixing energy varies with manure type and solids concentration for a given mixing time [41].

The actual mixing system, as documented in the fabrication drawings and field photographs, consists of two vertical shafts, each equipped with a stainless-steel marine propeller driven from above through a geared motor. The gearbox provides the low output rotational speed required to maintain the propeller within the prescribed power budget while preserving efficient axial pumping. The impeller diameter ($D = 0.25$ m) and the gearbox output rotational speed ($N = 4$ rev s^{-1}, i.e., 240 rpm) were taken directly from the fabrication drawings and are introduced as design inputs in the Section 3.

2.7. Biogas Production and Energy Potential

The theoretical methane production rate at reactor scale is given by $\dot{V}_{CH_4}^{th} = \mathrm{BMP}_{th} \cdot (\mathrm{VS} \cdot M)$. The realized methane and biogas production rates are obtained through the realization factor η_{bio} and the methane fraction x_{CH_4}, shown in Equation (9):

$$\dot{V}_{CH_4} = \eta_{bio}\, \dot{V}_{CH_4}^{th}, \qquad \dot{V}_{biogas} = \frac{\dot{V}_{CH_4}}{x_{CH_4}}. \tag{9}$$

The available thermal energy and the recoverable electrical energy in a generator set with efficiency η_e are given by $E_{th} = \dot{V}_{CH_4}\,\mathrm{LHV}_{CH_4}$ and $E_{el} = \eta_e E_{th}$, where $\mathrm{LHV}_{CH_4} = 10$ kWh m^{-3}. Since E_{el} scales linearly with η_{bio}, the net energy criterion (Section 2.8) is evaluated parametrically with respect to η_{bio}.

2.8. Net Energy Balance and Duty Cycle Calculation

The parasitic energy demand of mixing is expressed as an explicit function of the duty cycle δ. The two motors are treated according to their operating mode: the two internal gear motors, with combined power P_{mix}, perform operational mixing and operate at duty cycle δ, while the separate 0.75 kW inlet motor operates intermittently during feeding events only, contributing a fixed energy term E_{entry}. Thus, as shown in Equation (10),

$$E_{par}(\delta) = f_L\, P_{mix}\, \delta \cdot 24 + E_{entry}, \qquad E_{net}(\delta) = E_{el} - E_{par}(\delta), \tag{10}$$

where $f_L \in (0, 1]$ is the load factor ($f_L = 1$ is the conservative nameplate-based assumption). The energy-neutral duty cycle is therefore Equation (11):

$$\delta^* = \frac{E_{el} - E_{entry}}{f_L\, P_{mix} \cdot 24}. \tag{11}$$

It is explicitly noted that P_{mix} is a design assumption ($P_{mix} = 0.74$ kW, two units of 0.37 kW each), reported parametrically in order to allow substitution with measured values when available.

2.9. Substrate-Driven PLC Control Design (SD-PLC Methodology)

The central methodological contribution is a reproducible procedure that derives PLC timing setpoints directly from measured substrate properties, rather than adopting fixed default or literature-based mixing intervals. Existing PLC implementations typically define mixing timers empirically or via generic recommendations; here, each timing output is explicitly mapped to a physical property of the sludge. The procedure is structured in the stages shown in Figure 2 and uses the control variables listed in Table 1.

Table 1. PLC control variables of the SD-PLC methodology, their units and their substrate-driven origin.

Variable	Type	Unit	Origin/Setpoint Rule
Level (L_{high}, L_{low})	Input	m	Working volume limits; dry-run and overflow protection
pH	Input	–	Biological gate: inhibits operation if pH $<$ pH$_{min}$
EC	Input	mS cm^{-1}	VFA/salinity proxy: inhibits if EC $>$ EC$_{max}$
Temperature	Input	°C	Scales $\mu_{app}(T)$ and thus $t_{on,h}$; process health indicator
Feed flow (Q_{in})	Input	m^3 d^{-1}	Reconstructed as $A_{ch}\Delta L/t_{feed}$; confirms the loading event and supplies the on-line OLR estimate to the Stage 6 check
Dome pressure (p_{dome})	Input (diag.)	mbar	Qualitative gas-production watchdog; raises an alarm, does not gate the contactor
$t_{on,h}$	Calculated	min	Stage 2: homogenization time (rheology + geometry)
$t_{on,m}$, $t_{off,m}$	Calculated	min	Stages 3–5: bounded by $\min(t_{strat}, t_{cont})$ and by δ^*
δ	Calculated	–	$\sum t_{on}/24$ h; must satisfy $\delta_{min} \le \delta \le \delta^*$
t_{feed}	Calculated	min	Inlet motor timing linked to the feeding event
F_{col}	Internal	–	Collapse latch: set if pH $<$ pH$_{min}$ persists longer than t_{col}; inhibits feeding, alarms, manual reset
Inlet motor	Output	–	Load homogenization (event-based)
Gear motors	Output	–	Maintenance and homogenization pulses

Stage 0—Characterization inputs. Proximate/ultimate analysis (→VM, C/N, BMP$_{th}$; Section 2.3) and rheology (K, n, τ_0, μ_{app}, ρ; Section 2.5).

Stage 1—Separation of mixing objectives. The control law distinguishes: (a) homogenization of fresh feed after each loading event, and (b) maintenance mixing to prevent stratification/sedimentation between feedings. Their relative weighting depends on yield

stress τ_0 and density contrast $\Delta\rho$: a high τ_0 keeps fines in suspension and minimizes maintenance requirements, whereas a low τ_0 requires frequent mixing pulses.

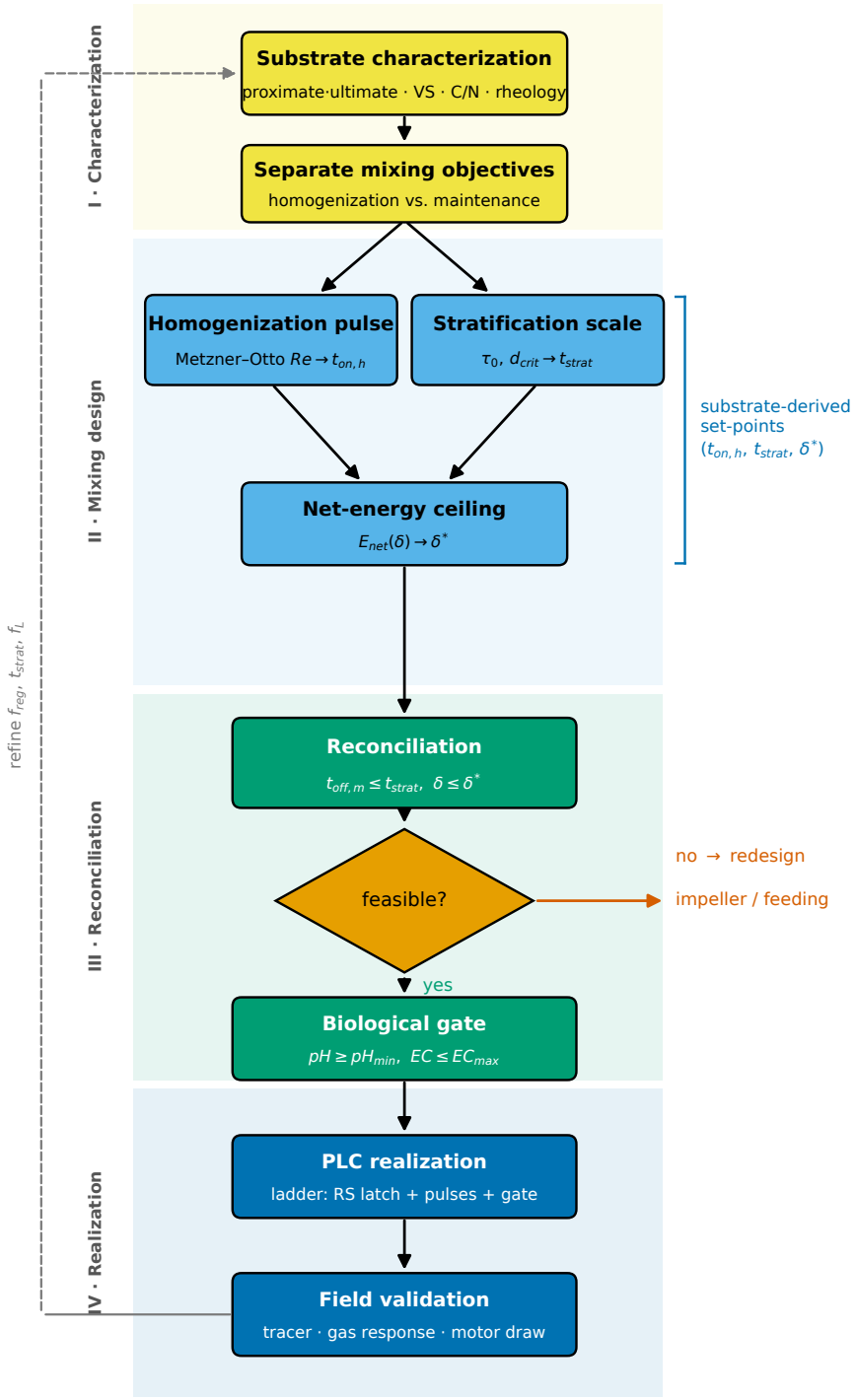

Figure 2. Substrate-Driven PLC Control Design (SD-PLC) methodology: Each timing setpoint is derived from a measured substrate property, reconciled against a net energy ceiling, and conditioned by biological safety before implementation in the PLC system.

Stage 2—Flow regime and homogenization time. The apparent viscosity evaluated at the impeller shear rate (Metzner–Otto approach) determines *Re* and the flow regime. The homogenization pulse duration is defined from the circulation time, shown in Equation (12):

$$t_{on,h} = n_c \, f_{reg}(Re) \, \frac{V_L}{N_Q \, N \, D^3}, \tag{12}$$

where V_L is the liquid working volume, N_Q is the pumping number, N is the rotational speed, D is the impeller diameter, n_c is the number of tank turnovers required to reach the target homogeneity ($n_c = 4$, i.e., $1 - e^{-n_c} \approx 98\%$ of the asymptotic homogeneity), and $f_{reg} \geq 1$ is a regime penalty factor that increases as Re decreases. The use of two impellers doubles the effective pumping capacity $N_Q N D^3$.

Stage 3—Maintenance interval: stratification and contact criteria. The maximum OFF interval is bounded by two independent physical constraints, $t_{off,m} \leq \min(t_{strat}, t_{cont})$.

The first is gravitational. In a yield-stress medium a particle remains indefinitely suspended when the gravitational yield number $Y_g = \tau_0 / (\Delta\rho \, g \, d_p)$ exceeds a critical value $Y_{g,crit}$, reported in the range 0.14–0.21 for a sphere in a Bingham fluid. This defines a critical suspension diameter, shown in Equation (13):

$$d_{crit} = \frac{\tau_0}{Y_{g,crit} \, \Delta\rho \, g}. \tag{13}$$

Taking $Y_{g,crit} = 0.2$ and a solid–liquid density contrast $\Delta\rho \approx 200\ \mathrm{kg\,m^{-3}}$, Equation (13) yields the compact sensitivity $d_{crit}\,[\mathrm{mm}] \approx 2.5\,\tau_0\,[\mathrm{Pa}]$. If $d_p < d_{crit}$ the fines do not settle and $t_{strat} \to \infty$; otherwise the hindered settling velocity and the stratification time over a fraction ϕ of the usable height H are shown in Equation (14):

$$v_s = \frac{\Delta\rho \, g \, d_p^2}{18 \, \mu_{app}} \left(1 - \frac{d_{crit}}{d_p}\right), \qquad t_{strat} = \frac{\phi \, H}{v_s}. \tag{14}$$

This is a single closure of the suspension criterion: the elementary force balance $(\pi/6) d_p^3 \Delta\rho g \leq \pi d_p^2 \tau_0$ provides the alternative estimate $d_{crit} = 6\tau_0/(\Delta\rho g)$, numerically equivalent to Equation (13) within the reported spread of $Y_{g,crit}$, and the two must not be combined.

The second constraint is non-gravitational and, unlike the first, can be closed with the parameters already available. Substrate–biomass segregation follows Equation (21); imposing a target segregation index $\Theta \leq \Theta_{tgt}$ on its quasi-steady solution $\Theta = k_{seg}/(k_{seg} + k_{mix}\delta)$ yields a minimum admissible duty cycle and hence a maximum OFF interval, shown in Equation (15):

$$\delta_{min} = \frac{k_{seg}}{k_{mix}} \, \frac{1 - \Theta_{tgt}}{\Theta_{tgt}}, \qquad t_{cont} = t_{on,m} \left(\frac{1440 - t_{on,h}}{1440 \, \delta_{min} - t_{on,h}} - 1 \right), \tag{15}$$

with all times expressed in minutes per day. This criterion is what converts the maintenance interval from a provisional rule into a computed setpoint. The yield stress τ_0 remains necessary, but its role is now to establish which of the two constraints binds, rather than to unblock the design.

Stage 4—Net energy ceiling. The duty cycle is constrained by the criterion in Section 2.8: $\delta = \sum t_{on} / 24\,\mathrm{h} \leq \delta^*$.

Stage 5—Reconciliation. The maintenance pair $(t_{on,m}, t_{off,m})$ is selected to simultaneously satisfy $t_{off,m} \leq \min(t_{strat}, t_{cont})$ (physical constraints) and $\delta_{min} \leq \delta \leq \delta^*$ (contact floor and energy ceiling). If the physical constraints enforce $\delta > \delta^*$, the substrate demands more mixing than allowed by the energy budget, and the method signals the need for a redesign of the impeller or feeding strategy rather than violating either constraint.

Stage 6—Biological gate. Mixing is enabled only within a safe operating window defined by acid–base behavior: $\mathrm{pH} \geq \mathrm{pH}_{min}$, $\mathrm{EC} \leq \mathrm{EC}_{max}$, temperature and level within admissible ranges. Given that the manure/organic waste mixture exhibits a low C/N ratio

(19.2) and a sensitive acidogenic start-up phase, excessive agitation during acidification would disperse methanogenic aggregates. The gate therefore suppresses or attenuates mixing when pH/EC indicators signal acid accumulation.

The feeding flow rate Q_{in} is incorporated as an input of the gate. It is not measured with a dedicated flowmeter—which would be prone to fouling and would exceed the cost envelope of the installation—but is reconstructed from the level transducer already installed in the inlet chamber as $Q_{in} = A_{ch}\Delta L/t_{feed}$, where A_{ch} is the chamber cross-sectional area and ΔL the level drop recorded during the feeding event. This provides an on-line estimate of the organic loading rate, $\mathrm{OLR} = Q_{in}S_{in}/V_L$, which serves two purposes: it confirms that a loading event has actually occurred before the homogenization pulse is released, preventing the agitator from running on an unfed reactor, and it supplies the supervisory layer with the variable that discriminates a transient acid shock from sustained organic overloading—the latter lying outside the scope of the mixing logic (Section 2.11).

Stage 7—PLC implementation. The reconciled setpoints are mapped onto a *ladder* program: a master set–reset (RS) latch, a feeding sequence (inlet motor t_{feed} followed by a homogenization pulse $t_{on,h}$), an asynchronous pulse generator for the maintenance sequence $(t_{on,m}, t_{off,m})$, and comparator blocks implementing the Stage 6 gate on all outputs prior to the contactors. Figure 3 presents the hierarchical control architecture and the corresponding *ladder* program: the agitator contactor output ($K_{agitator}$) is activated only when the temporal logic (homogenization or maintenance pulse) coincides with the stability gate condition ($\mathrm{pH} \geq \mathrm{pH}_{min}$, $\mathrm{EC} \leq \mathrm{EC}_{max}$, level within range). The program additionally implements a collapse latch F_{col}, described in Section 4.2, which converts a persistent gate violation into a safe stop.

Stage 8—Field validation. Homogeneity (tracer or EC uniformity), gas response, and motor power consumption are measured to refine f_{reg}, t_{strat}, and f_L.

2.10. Selection of Control Variables and Supervisory Law

The proposed methodology adopts process stability as the governing objective function—preventing process collapse due to acidification or ammonia inhibition—and subordinating methane production to it, since in rural digesters the dominant failure mode is instability rather than suboptimal yield. Under this criterion, control variables are selected not only based on their influence on process dynamics, but also on the product of their influence and their rural sensing feasibility. Each candidate variable v is assigned a weighted score, shown in Equation (16):

$$S(v) = \sum_k w_k\, s_k(v), \qquad \sum_k w_k \;=\; 1, \tag{16}$$

over five criteria k: process sensitivity, low sensor cost, field robustness, absence of consumables or low calibration demand, and actuation relevance.

The weights prioritize stability and rural feasibility and are fixed at $w = (0.30, 0.20, 0.20, 0.15, 0.15)$ respectively, so that process sensitivity dominates while sensor cost and field robustness jointly carry an equal weight. A variable enters the control set when $S(v) \geq 3.5$; this threshold is stated explicitly so that the selection and ranking of variables can be reproduced or re-weighted by the reader. Highly informative but low-feasibility variables—such as volatile fatty acids determined by titration or chromatography and alkalinity determined by titration—fall below this threshold.

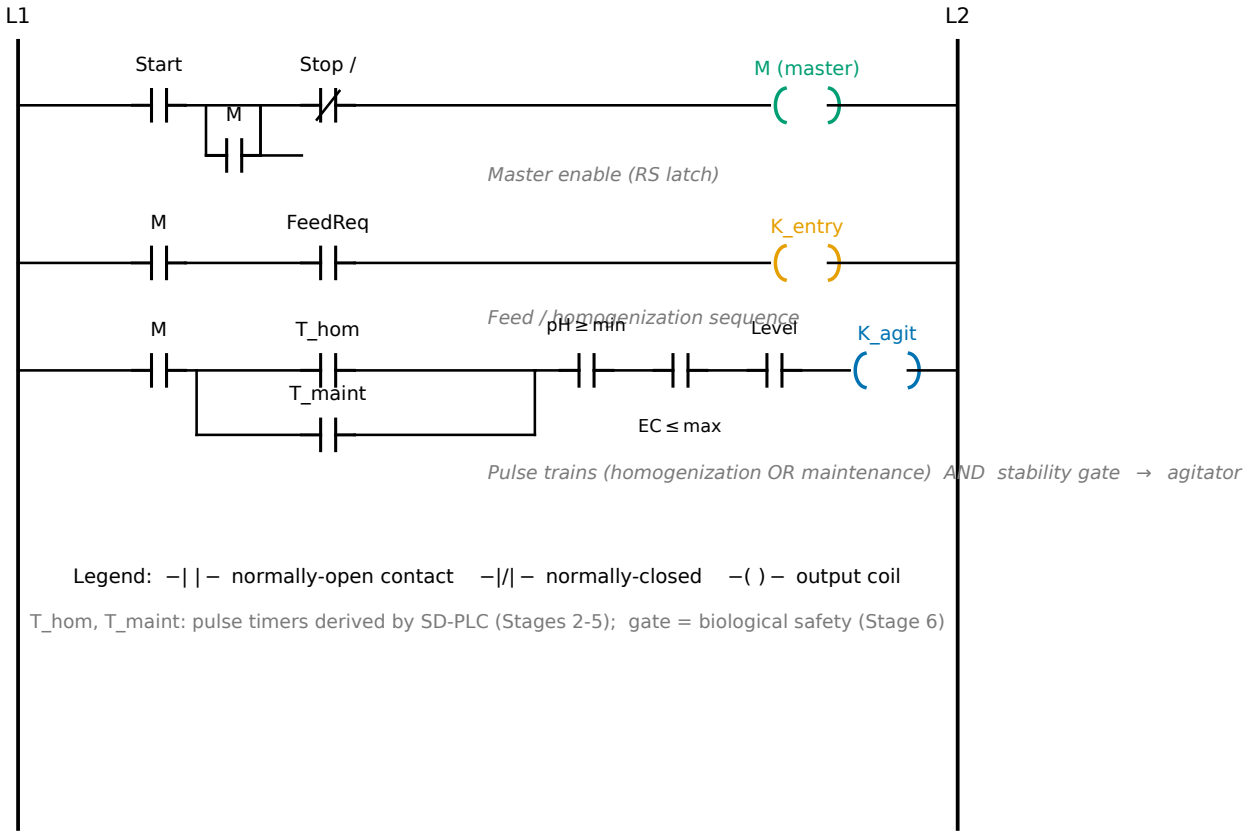

Figure 3. PLC programming and control system architecture. Hierarchical control architecture (field–control–supervisory layers) with a 24 VDC backup power supply, together with the SD-PLC ladder program integrating the master latch, feeding sequence, homogenization and maintenance pulse generators, the collapse latch, and the pH/EC/level stability gate governing the agitator contactor signal.

The resulting control law couples a substrate-driven feedforward program (Stages 2–5) with a feedback supervisory layer based on the selected variables. Mixing is enabled as a logical conjunction between the temporal program and stability gates, shown in Equation (17):

$$u_{ag}(t) = f_{prog}(t) \ \wedge \ (\mathrm{pH} \geq \mathrm{pH}_{min}) \ \wedge \ (\mathrm{EC} \leq \mathrm{EC}_{max}) \ \wedge \ (L_{low} \leq L \leq L_{high}), \tag{17}$$

where $f_{prog}(t)$ is the binary output of the feedforward timing program of Stages 2–5 and L is the measured liquid level, while temperature rescales the homogenization pulse duration through the temperature dependence of apparent viscosity (Arrhenius-type behavior), shown in Equation (18):

$$t_{on,h}(T) = t^0_{on,h}\left[\frac{\mu_{app}(T)}{\mu^0_{app}}\right]^m, \qquad \mu_{app}(T) = \mu^0_{app}\exp\left[\frac{E_\mu}{R_g}\left(\frac{1}{T} - \frac{1}{T_0}\right)\right], \tag{18}$$

where E_μ is the viscous activation energy, R_g is the gas constant, and m is the sensitivity exponent of mixing time to viscosity. Neither E_μ nor m has been determined for this slurry; the rescaling is therefore specified as part of the methodology but is not instantiated numerically in the present case study, and its calibration is listed in Stage 8 together with f_{reg} and f_L. Thus, temperature governs how much to mix, while pH, EC, and level govern when mixing is allowed. The complete structure is summarized in the control loop shown in Figure 4.

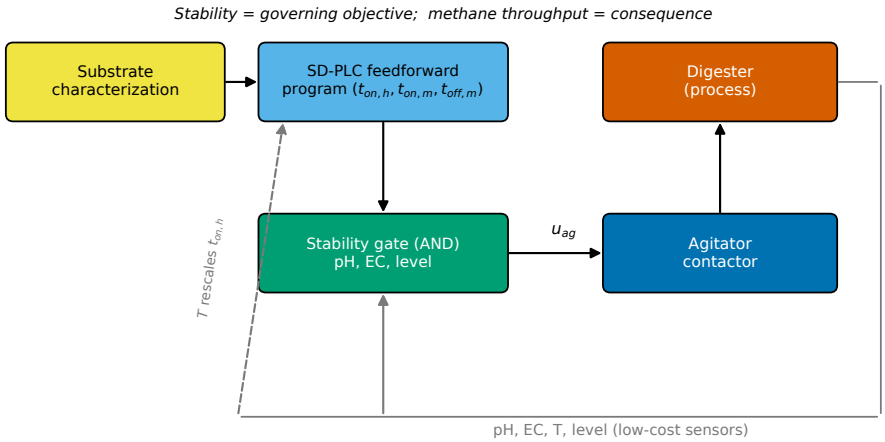

Figure 4. Control architecture: Substrate-Driven Feedforward PLC Design (SD-PLC) coupled with a low-cost feedback supervisory layer. Temperature rescales $t_{on,h}$, while pH, EC, and level enable or inhibit the agitator contactor signal. Stability is the governing objective function, with production treated as a consequence.

2.11. Closed-Loop Dynamic Modeling

To evaluate controller behavior under perturbations, a closed-loop dynamic model was implemented in Python v 3.12 using a reduced COD-based anaerobic digestion model with two stages (hydrolysis/acidogenesis and methanogenesis) coupled to mixing dynamics.

The choice of a two-stage structure instead of ADM1 is deliberate and follows the control-oriented modeling tradition. ADM1 comprises 24 dynamic state variables and 19 biochemical processes with of the order of one hundred stoichiometric and kinetic parameters [42]; with the instrumentation available in a rural fixed-dome digester—pH, electrical conductivity, temperature, level and daily gas volume—that parameter set is neither identifiable nor the state vector observable, and a non-identifiable model cannot support a control-design argument. Reduced two-step structures were developed precisely for this purpose: AM2 [43] describes acidogenesis and methanogenesis with six states and remains a reference model for observer and controller synthesis in anaerobic digestion, and its extension AM2HN [44] adds hydrolysis and ammoniacal nitrogen; recent assessments confirm that reduced-order structures are the appropriate choice when real-time implementation is the objective [45].

Two clarifications are necessary. First, the acid–base behaviour on which the controller acts is not simplified: the carbonate buffer (Equation (19)) and the ADM1 pH inhibition function (Equation (20)) are retained without modification, so the gating logic is evaluated against an ADM1-consistent description of acidification. Second, the model extends rather than merely reduces the standard structures, because the manipulated variable of this work is agitation and neither ADM1 nor AM2 contains a state describing floc integrity or substrate–biomass contact; the states R and Θ (Equations (21) and (22)) were therefore added. The model is consequently not a competitor of ADM1 in predictive accuracy: it is the minimal structure containing the two failure mechanisms the controller must arbitrate—shear damage and contact deficit—and nothing beyond them. Accordingly it does not resolve acetogenesis, hydrogen partial pressure, long-chain fatty acid inhibition, free-ammonia inhibition or sulfate reduction, and no conclusion drawn from the simulations invokes those mechanisms.

The model is intended as a behavioral representation of control performance rather than a calibrated predictive biogas model; its purpose is to compare relative stability under different agitation strategies. The steady-state reference is anchored to the measured field production of the reactor ($\approx$3.4 m^3 CH$_4$ d^{-1}, $\eta_{bio} \approx 0.21$). State variables include biodegradable particulate COD X_s, volatile fatty acids expressed as COD S_a and methanogenic

biomass X_m (all per unit liquid volume), together with the dimensionless aggregate integrity $R \in [0,1]$ and segregation index $\Theta \in [0,1]$. Temperature dependence of reaction rates, normalized at 35 °C, follows $f_T(T) = \exp[0.069(T-35)]$.

Two conventions must be stated to make the parameter set of Table 2 traceable to the field data of Table 3. The influent term $S_{in} = 37.1$ g COD L^{-1} is the biodegradable COD, that is, the total influent COD (≈180 g COD L^{-1} for a volatile solids concentration of 126.9 g VS L^{-1}) already scaled by the realization factor $\eta_{bio} \approx 0.21$; the model therefore reproduces the observed production without claiming to predict η_{bio} itself. In addition, biomass decay is not returned to the particulate pool, and the residual COD imbalance associated with this open term is the source of the closure error reported below.

Bicarbonate buffer and pH. Unlike empirical pH–VFA correlations, pH is explicitly coupled to carbonate buffering. With VFA converted to milliequivalents $S_a^{\mathrm{meq}} = S_a(1000/64)$ (64 g COD mol^{-1} as acetate equivalent) and residual bicarbonate alkalinity $A_b = \max(A_T - S_a^{\mathrm{meq}}, \varepsilon)$, as shown in Equation (19),

$$\mathrm{pH} = \mathrm{p}K_a + \log_{10}\left(\frac{A_b}{A_{\mathrm{CO_2}}}\right), \tag{19}$$

with $\mathrm{p}K_a = 6.3$ and $A_{\mathrm{CO_2}}$ representing dissolved CO_2 reference alkalinity. Methanogenic inhibition due to low pH follows the ADM1 formulation [42], shown in Equation (20):

$$I_{\mathrm{pH}} = \exp\left[-3\left(\frac{\mathrm{pH}-\mathrm{pH}_{UL}}{\mathrm{pH}_{UL}-\mathrm{pH}_{LL}}\right)^2\right], \quad (\mathrm{pH} < \mathrm{pH}_{UL}), \qquad I_{\mathrm{pH}} = 1 \ (\mathrm{pH} \geq \mathrm{pH}_{UL}), \tag{20}$$

with a corresponding acidogenesis inhibition term I_{pH}^h (more tolerant to acidic conditions) based on Veeken et al. [46].

Mixing coupling: Contact benefit vs. shear damage. Mixing produces two competing physical effects. First, stagnation leads to segregation—loss of substrate–biomass contact and formation of local acidogenic microenvironments—which mixing mitigates, shown in Equation (21):

$$\frac{d\Theta}{dt} = k_{seg}(1-\Theta) - k_{mix}u_{ag}\Theta, \qquad \eta_c = 1 - \lambda\Theta, \tag{21}$$

where $u_{ag} \in \{0,1\}$ is the agitation signal and η_c is the contact efficiency scaling methanogenesis. Here, Θ does not represent gravitational stratification (negligible due to yield stress effects, $d_p < d_{crit}$, $t_{strat} \to \infty$; Stage 3), but rather non-gravitational heterogeneity of contact [47]. Second, under acid stress, methanogenic aggregates are fragile and shear induces disintegration [15,16,48,49]. With acid stress index

$$\sigma = \mathrm{clip}\left[\frac{(S_a^{\mathrm{meq}}/A_T - \rho_{lo})}{(\rho_{hi} - \rho_{lo})}, 0, 1\right],$$

where $\mathrm{clip}[x,0,1]$ denotes saturation of x to the interval $[0,1]$ (Ripley ratio formulation), aggregate integrity evolves as Equation (22):

$$\frac{dR}{dt} = -k_{sh}(1+\gamma\sigma)u_{ag}R + k_{rec}(1-R)I_{\mathrm{pH}}, \tag{22}$$

so that agitation under acidic conditions ($\sigma \to 1$) accelerates deterioration, while recovery occurs as pH stabilizes.

Kinetics and mass balances. Hydrolysis and methanogenesis rates are shown in Equation (23):

$$r_{hyd} = k_{hyd}f_T I_{\mathrm{pH}}^h X_s, \qquad r_m = k_m f_T \eta_c I_{\mathrm{pH}} R \frac{S_a}{K_S + S_a} X_m, \tag{23}$$

with mass balances (including biomass retention and semi-continuous feeding at dilution rate $D_h = 1/\mathrm{HRT}$), shown in Equations (24)–(26):

$$\frac{dX_s}{dt} = D_h(S_{in} - X_s) - r_{hyd}, \tag{24}$$

$$\frac{dS_a}{dt} = r_{hyd} - r_m - D_h S_a + \Delta_a \delta_D(t - t^*), \tag{25}$$

$$\frac{dX_m}{dt} = Y_x r_m - k_d X_m, \tag{26}$$

where $\Delta_a \delta_D(t - t^*)$ represents an acid shock event, and δ_D denotes the Dirac distribution and not the duty cycle δ. Methane production is $Q_{\mathrm{CH_4}} = Y_{\mathrm{CH_4}}(1 - Y_x) r_m V_L$, the factor $(1 - Y_x)$ excluding the COD fraction diverted to biomass synthesis.

The controller implements the law defined in Section 2.10: mixing is enabled to maintain contact ($\Theta \leq \Theta_{tgt}$), but inhibited by the stability gate ($u_{ag} = 0$ if pH or Ripley ratio thresholds are violated), thereby protecting R. Parameters (Table 2) are drawn from anaerobic digestion and mixing literature; COD closure was numerically verified (error $< 5\%$).

Table 2. Parameters of the illustrative dynamic model (literature-based values; steady-state anchored at ≈3.4 $\mathrm{m^3\,CH_4\,d^{-1}}$).

Group	Parameter (Symbol)	Value	Unit
Reactor/operation	Liquid working volume (V_L), HRT	10.5, 30	$\mathrm{m^3}$, d
	Temperature (T)	22.5	°C
	Influent biodegradable COD (S_{in})	37.1	$\mathrm{g\,COD\,L^{-1}}$
Kinetics	Hydrolysis (k_{hyd})	0.30	$\mathrm{d^{-1}}$
	Methanogenesis (k_m, K_S)	8.0, 1.0	$\mathrm{d^{-1}}$, $\mathrm{g\,COD\,L^{-1}}$
	Yield/decay (Y_x, k_d)	0.05, 0.02	–, $\mathrm{d^{-1}}$
	Methane yield ($Y_{\mathrm{CH_4}}$)	0.35	$\mathrm{L\,CH_4\,g\,COD^{-1}}$
Buffer/pH	Alkalinity, CO_2 reference (A_T, $A_{\mathrm{CO_2}}$)	70, 6	$\mathrm{meq\,L^{-1}}$
	ADM1 thresholds (pH_{UL}, pH_{LL})	7.0, 6.0	–
Mixing/shear	Homogenization/segregation (k_{mix}, k_{seg})	48, 2.5	$\mathrm{d^{-1}}$
	Contact loss (λ)	0.60	–
	Shear/repair (k_{sh}, γ, k_{rec})	0.15, 18, 0.35	$\mathrm{d^{-1}}$, –, $\mathrm{d^{-1}}$
Controller	Gate (pH_{min}, Ripley max, Θ_{tgt})	6.60, 0.60, 0.30	–

Scope of the test. The evaluated disturbance is a transient acid shock, which is precisely the instability mode targeted by the supervisory gate. Sustained organic overloading is explicitly excluded, as its correct response requires feed management rather than mixing control. A gate that suppresses mixing under persistent acidity would be counterproductive under sustained overload, which belongs to a higher-level control layer.

Table 3. Input data of the case study (measured substrate composition and design parameters). All subsequent calculations are derived exclusively from these values.

Group	Parameter (Symbol)	Value	Unit
Substrate (measured)	Moisture RO/GP (W)	87.89/27.51	%
	Volatile matter RO/GP (VM)	11.79/58.40	% wet basis
	C, H, N, O, S RO	38.80, 6.00, 3.47, 51.73, 0	%
	C, H, N, O, S GP	42.30, 6.00, 2.10, 49.60, 0	%

Table 3. *Cont.*

Group	Parameter (Symbol)	Value	Unit
Operation	Daily feed mass (M)	100	kg d^{-1}
	Dilution water (M_w)	264	kg d^{-1}
	Co-digestion ratio (RO:GP)	30:70	–
	Hydraulic retention time (HRT)	30	d
	Overdesign factor (f_{sv})	1.30	–
	Mixture density (ρ)	1040	kg m^{-3}
Geometry	Length, width, height (l, a, h)	2.46, 2.92, 1.93	m
	Impeller diameter (D) †	0.25	m
	Number of impellers	2	–
Mixing/energy	Apparent viscosity (μ_{app})	0.05–0.80	Pa s
	Pumping number (N_Q)	0.5	–
	Impeller speed (N) †	4	rev s^{-1}
	Circulation cycles/penalty (n_c, f_{reg})	4, 2	–
	Mixing power (P_{mix}) ‡	0.74	kW
	LHV$_{CH_4}$, η_e	10, 30	kWh m^{-3}, %

† Taken from the fabrication drawings (Section 2.6); pending confirmation by direct measurement during the field validation campaign (Stage 8). ‡ Nameplate rating; the effective load factor f_L is to be determined from motor power monitoring.

3. Results

3.1. Input Data

All subsequent calculations are derived from a single unified set of input data summarized in Table 3: the measured substrate composition (proximate/ultimate analysis), reactor operating and geometric parameters, and mixing and energy parameters. Values taken from the fabrication drawings (D, N) and nameplate ratings (P_{mix}) are flagged and propagated as such throughout the sensitivity analysis.

3.2. Substrate Characterization and Theoretical Methane Potential

From the proximate and ultimate analyses in Table 3, guinea pig manure exhibits a substantially higher volatile matter content (VM = 58.4% wet basis) than organic residues (VM = 11.8%), with elemental C/N ratios of 20.1 and 11.2, respectively. The resulting empirical formulas (normalized per N) are $C_{13}H_{24}O_{13}N$ for organic residues and $C_{23.5}H_{39.7}O_{20.7}N$ for guinea pig manure.

Applying the Buswell–Boyle stoichiometry, the theoretical methane potentials are 375 mL CH_4 g^{-1} VS (manure, 47.5% CH_4) and 327 mL CH_4 g^{-1} VS (residues, 45.1% CH_4). Table 4 and Figure 5 show the co-digestion series: both volatile matter content and theoretical methane per unit fresh mass increase monotonically with the fraction of manure. The preliminary design mixture (30:70) maximizes both VM (44.4%) and methane yield per fresh mass (164.9 L CH_4 kg^{-1} fresh), with a weighted BMP$_{th}$ of 371 mL CH_4 g^{-1} VS and C/N = 19.2.

It is important to state explicitly that, based on these two indicators alone, monodigestion of manure would score higher (VM = 58.4%; C/N = 20.1, closer to the optimal range of 20–30). Organic residues, in fact, dilute both performance indicators. Moreover, the stoichiometric analysis shows that organic residues contribute a higher potential nitrogen load (3.47 vs. 2.10 g N per 100 g VS), increasing the risk of ammonia inhibition.

Therefore, the rationale for co-digestion is not the maximization of VM or C/N, but two explicitly design-driven criteria: (i) the valorization of an otherwise unmanaged organic waste stream (waste management objective), and (ii) its function as a highly hydrated

diluent (W = 87.9%) that reduces external water demand. This is a design decision, not a performance optimum.

Table 4. Co-digestion mixtures (RO:GP by fresh mass): C/N ratio, volatile matter, and theoretical methane potential (Buswell–Boyle).

RO:GP	C/N	VM (% Wet)	BMP_{th} (mL CH_4 g^{-1} VS)	Theoretical CH_4 (L kg^{-1} Fresh)
70:30	16.63	25.77	360	92.7
60:40	17.52	30.43	364	110.7
50:50	18.20	35.10	367	128.8
40:60	18.75	39.76	369	146.9
30:70	19.19	44.42	371	164.9

C/N is computed on a dry-matter basis, following the convention of the anaerobic digestion literature, whereas VM and BMP_{th} are weighted by volatile solids.

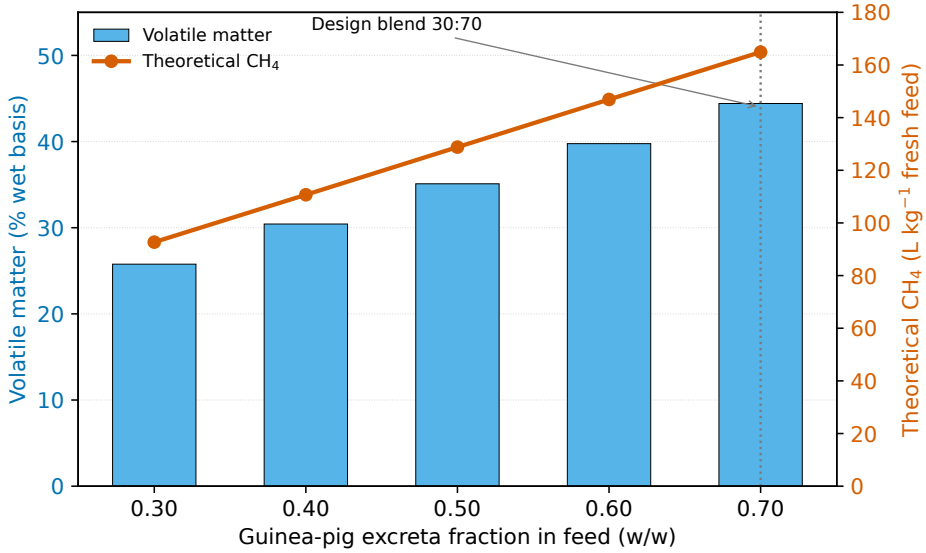

Figure 5. Volatile matter (wet basis) and theoretical methane potential (Buswell–Boyle) as a function of RO:GP co-digestion ratio. Both indicators increase with manure fraction; the preliminary design mixture (30:70) is highlighted.

3.3. Rheological Properties and Mixing Regime

The installed mixing configuration ($D = 0.25$ m, $N = 4$ rev s^{-1}, two impellers, combined nameplate power $P_{mix} = 0.74$ kW) gives an impeller Reynolds number, shown in Equation (27):

$$Re = \frac{\rho N D^2}{\mu_{app}} = \frac{260}{\mu_{app}}. \quad (27)$$

The operating point must be evaluated at a single, self-consistent dilution. From $Q = (M + M_w)/\rho$ with $M = 100$ kg d^{-1} and $M_w = 264$ kg d^{-1}, the feed corresponds to a mass dilution of approximately 1:2.6; accordingly, representative operating values of $\rho = 1040$ kg m^{-3} and $\mu_{app} = 0.10$–0.30 Pa s were adopted for the fed condition. The operating envelope is therefore $Re \approx 0.9$–2.6×10^3. Across the full range of dilutions considered, from 1:2 ($\rho = 1050$ kg m^{-3}, μ_{app} up to 0.80 Pa s) to 1:3 ($\rho = 1025$ kg m^{-3}, μ_{app} down to 0.05 Pa s), the extreme bounds are $Re \approx 3 \times 10^2$ to 5×10^3.

In every case the flow remains transitional and never reaches fully turbulent conditions. Consequently, classical turbulent power correlations are not directly applicable, and mixing is diffusion-limited near the vessel walls—consistent with persistent dead

zones and scum formation in fixed-dome digesters [11,16]. The regime map in Figure 6 confirms this conclusion: for the viscosity range of the substrate and the impeller diameters considered, the Reynolds number remains within the transitional band throughout the operating envelope.

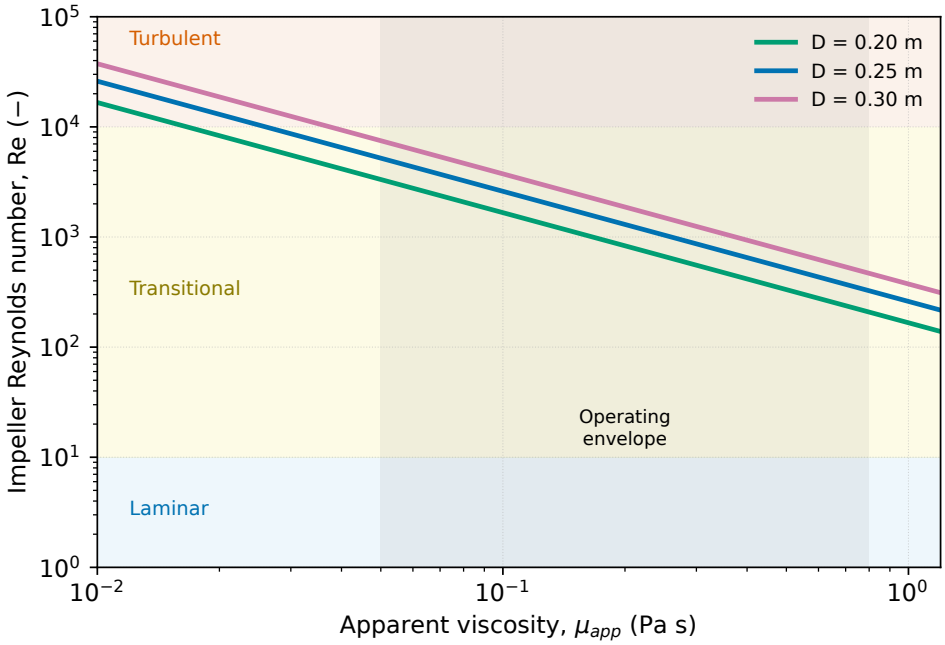

Figure 6. Hydrodynamic regime map: Impeller Reynolds number versus apparent slurry viscosity for three impeller diameters. The shaded regions indicate laminar, transitional, and turbulent regimes; the operating envelope remains entirely within the transitional regime.

The rotational speed deserves explicit justification, since it enters Equation (27) linearly and the power balance cubically. N is not a fitted parameter: it is the gearbox output speed of the installed drive (240 rpm), taken from the fabrication drawings together with D. Three independent checks confirm that it lies in a defensible region. First, the tip speed $v_{tip} = \pi ND = 3.14\,\mathrm{m\,s^{-1}}$ falls within the 3–5 $\mathrm{m\,s^{-1}}$ range recommended for axial impellers in digestion slurries. Second, with $P = N_p \rho N^3 D^5$ and N_p between ≈0.35 (turbulent correlation) and ≈2 (transitional regime), the hydraulic power of the two impellers is 46–260 W, that is 6–35% of the nameplate 0.74 kW, which confirms quantitatively that the installed power is governed by start-up torque and resuspension rather than by fully developed turbulence (Section 2.6). The associated Camp velocity gradient, shown in Equation (28),

$$G = \sqrt{\frac{P}{\mu_{app} V_L}}, \tag{28}$$

is 5–13 $\mathrm{s^{-1}}$ at $\mu_{app} = 0.15$ Pa s, a low-shear regime consistent with the preservation of methanogenic aggregates required by the stability-first objective. Third, the parametric sensitivity in Table 5 makes the trade-off explicit: increasing N shortens the homogenization pulse only in inverse proportion while raising the energy per pulse quadratically and the shear power cubically, whereas decreasing it drives Re towards the laminar boundary where the regime penalty f_{reg} grows and the circulation-time estimate loses reliability. A faster impeller would homogenize marginally sooner at the cost of the aggregate integrity that the control law exists to protect.

Table 5. Sensitivity of the mixing design to impeller rotational speed ($D = 0.25$ m, two impellers, $\mu_{app} = 0.15$ Pa s, $V_L = 10.5$ m^3). The installed value is shown in bold.

Quantity	$N = 2$	$N = 4$	$N = 6$	Scaling
Re (–)	867	**1733**	2600	$\propto N$
$t_{on,h}$ (min)	44.8	**22.4**	14.9	$\propto N^{-1}$
P, two impellers, $N_p = 0.35$ (W)	5.7	**45.5**	153.6	$\propto N^3$
G (s^{-1})	1.9	**5.4**	9.9	$\propto N^{3/2}$
Energy per pulse (Wh)	4.2	**17.0**	38.2	$\propto N^2$

Table 6 summarizes the density and apparent viscosity of guinea pig manure and its dilutions. The mixtures exhibit densities above 1000 kg m^{-3} and apparent viscosities one to three orders of magnitude higher than water, confirming a non-Newtonian pseudoplastic medium prone to sedimentation and stratification in the absence of forced mixing.

Table 6. Density and representative apparent viscosity of the substrate and its dilutions.

Material/Mixture	Condition/Ratio	Density (kg m^{-3})	Apparent Viscosity (Pa s)
Guinea pig manure	Fresh	1050–1100	0.5–3.0
Water	Ambient	1000	0.89×10^{-3}
Manure–water	1:3	1025	0.05–0.15
Manure–water (fed)	1:2.5	1040	0.10–0.30
Manure–water	1:2	1050	0.30–0.80

3.4. Energy Potential: Theoretical Versus Realized

The existing reactor satisfies the sizing criterion: using the data in Table 3, $Q = (M + M_w)/\rho \approx 0.35$ m^3 d^{-1}, $V_d = Q \cdot \mathrm{HRT} = 10.5$ m^3, and $V_{cd} = f_{sv} V_d = 13.65$ m^3, compared with a constructed volume $V = l\,a\,h = 13.86$ m$^3 \geq V_{cd}$, which justifies retaining the civil structure.

With a daily feed of 100 kg d^{-1} of the 30:70 mixture (volatile solids load = 44.4 kg d^{-1}) and $\mathrm{BMP}_{th} = 371$ mL CH_4 g^{-1} VS, the theoretical methane production rate is shown in Equation (29):

$$\dot{V}^{th}_{CH_4} = 16.5\ \mathrm{m^3 CH_4\,d^{-1}}, \tag{29}$$

representing the upper bound under complete conversion. In contrast, the field reactor achieves approximately 5.7 m^3 d^{-1} of biogas (approximately 3.4 m^3 CH_4 d^{-1} at ≈60% CH_4), corresponding to a realization factor $\eta_{bio} \approx 0.21$ (77 mL CH_4 g^{-1} VS). This low BDI is characteristic of low-mesophilic, poorly mixed operation [16,27,37] and quantifies the improvement potential targeted by the proposed redesign: increasing η_{bio} from ≈0.21 to the range 0.35–0.50 typical of well-mixed mesophilic digestion would double or triple production without changing the substrate. As discussed in Section 3.8, this projection rests on the elimination of dead zones and of the surface crust—that is, on an increase in the effectively active volume—and not on the contact mechanism represented in the dynamic model.

At baseline, the realized thermal energy is approximately 34 kWh d^{-1} and the electrical output about 10.3 kWh d^{-1} ($\eta_e = 30\%$). As a reference point, theoretical production ($\eta_{bio} = 1$) would correspond to the cooking energy demand of dozens of people in rural settings, where a large fraction of the Andean population lacks access to clean cooking fuels [27,28]. It is emphasized that the theoretical Buswell composition (47% CH_4) is lower than the commonly measured 55–65% range, since it assumes complete conversion of the entire elemental pool; both values are explicitly distinguished.

Figure 7 illustrates this gap: the theoretical methane ceiling, the realized field production, and the achievable target band resulting from an increased realization factor enabled by improved mixing control.

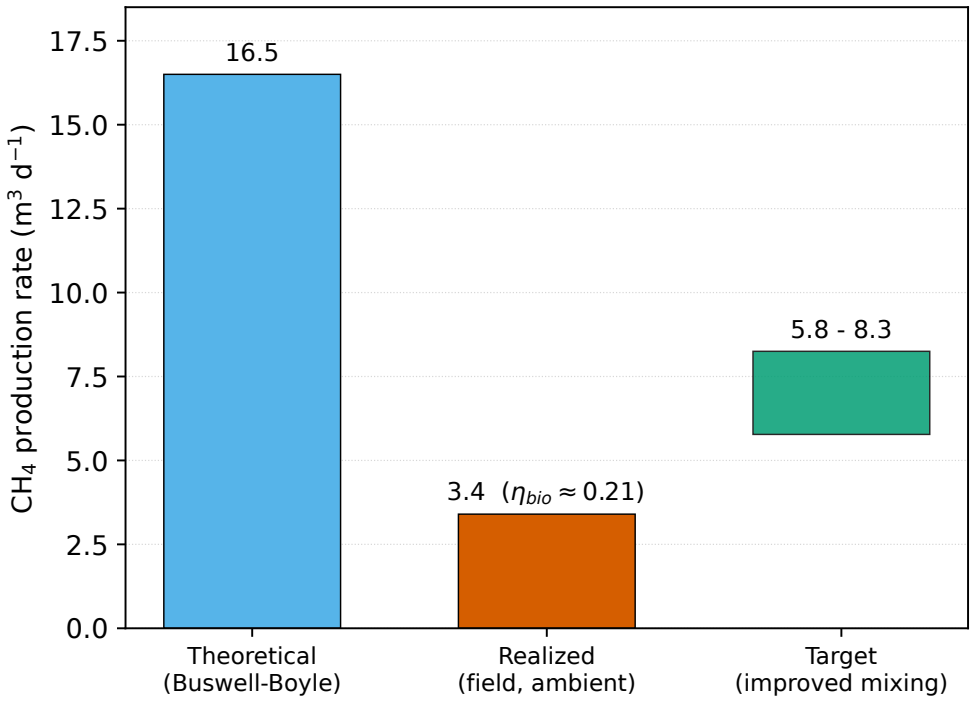

Figure 7. Methane production rate: Theoretical ceiling (Buswell–Boyle, complete conversion), realized field production of the reactor, and redesign target band (improved mixing). The target bar indicates the range associated with a realization factor of 0.35–0.50.

3.5. Net Energy Balance and Duty Cycle

With service mixing provided by two gearmotors ($P_{mix} = 0.74$ kW) and the feeding motor operating per event ($E_{entry} \approx 0.38$ kWh d^{-1}), the energy balance is expressed as $E_{net}(\delta) = 9.92 - 17.76\,\delta$ (nameplate-based). Continuous mixing ($\delta = 1$) requires 18.1 kWh d^{-1} and renders the plant energy-negative ($E_{net} = -7.8$ kWh d^{-1}), whereas the break-even point is $\delta^* = (10.3 - 0.38)/(0.74 \times 24) \approx 0.56$.

Figure 8 and Table 7 quantify this behavior. Importantly, this constraint is performance-dependent: it is restrictive in the baseline state ($\eta_{bio} \approx 0.21$), but relaxes as conversion efficiency increases—for $\eta_{bio} \gtrsim 0.37$, the recovered electrical energy exceeds even the demand of continuous mixing. Intermittent operation is therefore not justified by the energy argument alone; the independent yield evidence is discussed in Section 4.1.

Table 7. Net electrical balance as a function of duty cycle (nameplate basis, $f_L = 1$; $E_{el} = 10.3$ kWh d^{-1}). Base case: Two gearmotors $P_{mix} = 0.74$ kW plus feeding motor $E_{entry} = 0.38$ kWh d^{-1}. Conservative bound: 1.5 kW combined plus the same feeding term.

Regime	δ	E_{par} (Base)	E_{net} (Base)	E_{net} (Conservative)
Continuous	1.00	18.1	−7.8	−26.1
15 min h^{-1}	0.25	4.8	+5.5	+0.9
10 min h^{-1}	0.167	3.4	+7.0	+3.9
Reconciled program	0.124	2.6	+7.7	+5.5
5 min h^{-1}	0.083	1.9	+8.5	+6.9

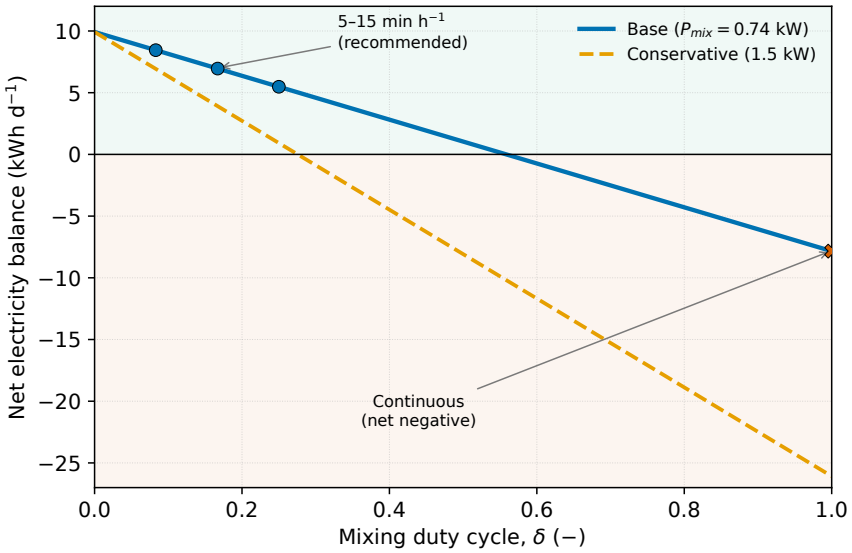

Figure 8. Net electrical balance as a function of mixing duty cycle (baseline $P_{mix} = 0.74$ kW and conservative upper bound 1.5 kW). The reconciled operating point ($\delta = 0.124$) remains net positive under both assumptions, while continuous mixing is strongly negative.

3.6. Control Program Derived from the SD-PLC Methodology

Applying the methodology of Section 2.9 to the Chillón reactor yields the timing program shown in Figure 9, rather than a literature-fixed interval. For the homogenization pulse (Stage 2), with a mixed volume $V_L = 10.5$ m^3, two marine impellers ($N_Q \approx 0.5$, $N = 4$ rev s^{-1}, $D = 0.25$ m), $n_c = 4$ and a transitional penalty $f_{reg} = 2$, the circulation time is $t_{circ} = V_L/(2N_Q N D^3) = 168$ s and $t_{on,h} = n_c f_{reg} t_{circ} \approx 22$ min. This value is highly sensitive to geometry: it ranges from ≈13 min ($D = 0.30$ m) to ≈44 min ($D = 0.20$ m), so D must be confirmed from the manufacturing drawings (Table 8 and Figure 10). By contrast, the dependence on the rotational speed is only first order (Table 5), which orders the priorities of the field validation campaign.

Table 8. Derived timing setpoints for the case study and sensitivity to impeller geometry.

Parameter	$D = 0.20$ m	$D = 0.25$ m	$D = 0.30$ m
Pumping $2N_Q N D^3$ (L s^{-1})	32.0	62.5	108.0
Circulation time t_{circ} (s)	328	168	97
Homogenization pulse $t_{on,h}$ (min)	43.7	22.4	13.0
Re ($\mu_{app} = 0.15$ Pa s)	1109	1733	2496

The maintenance interval follows from the reconciliation of Stages 3 to 5. The gravitational constraint cannot yet be evaluated numerically because τ_0 has not been measured, but the contact constraint can: with $k_{seg} = 2.5$ d^{-1}, $k_{mix} = 48$ d^{-1} and $\Theta_{tgt} = 0.30$, Equation (15) gives $\delta_{min} = 0.122$ and hence $t_{cont} \approx 42$ min. Selecting $t_{on,m} = 5$ min every $t_{off,m} = 40$ min—that is, 31 maintenance pulses per day once the post-feeding pulse has occupied part of the first cycle—yields $\delta = 0.124$, which satisfies the contact criterion ($\Theta = 0.297 \leq \Theta_{tgt}$) while remaining a factor of 4.5 below the energy ceiling $\delta^* \approx 0.56$ and leaving the plant net positive ($E_{net} = 7.7$ kWh d^{-1}, Table 7).

Energy is therefore not the active constraint: the binding limit is the contact criterion, and the gravitational limit t_{strat} will displace it only if the measured yield stress proves low enough for $d_p \geq d_{crit}$. The role of the pending rheological measurement is thus to establish which of the two constraints governs, not to unblock the design—a distinction that converts the maintenance schedule from a provisional interval into a computed setpoint.

The biological gate (Stage 6) suppresses agitation when pH falls below 6.6 (Figure 9). The resulting program—a long post-feeding homogenization pulse followed by short maintenance pulses, contact-bounded, energy-bounded and pH-conditioned—is the substrate-driven control output that a generic "5–15 min h^{-1}" rule cannot provide.

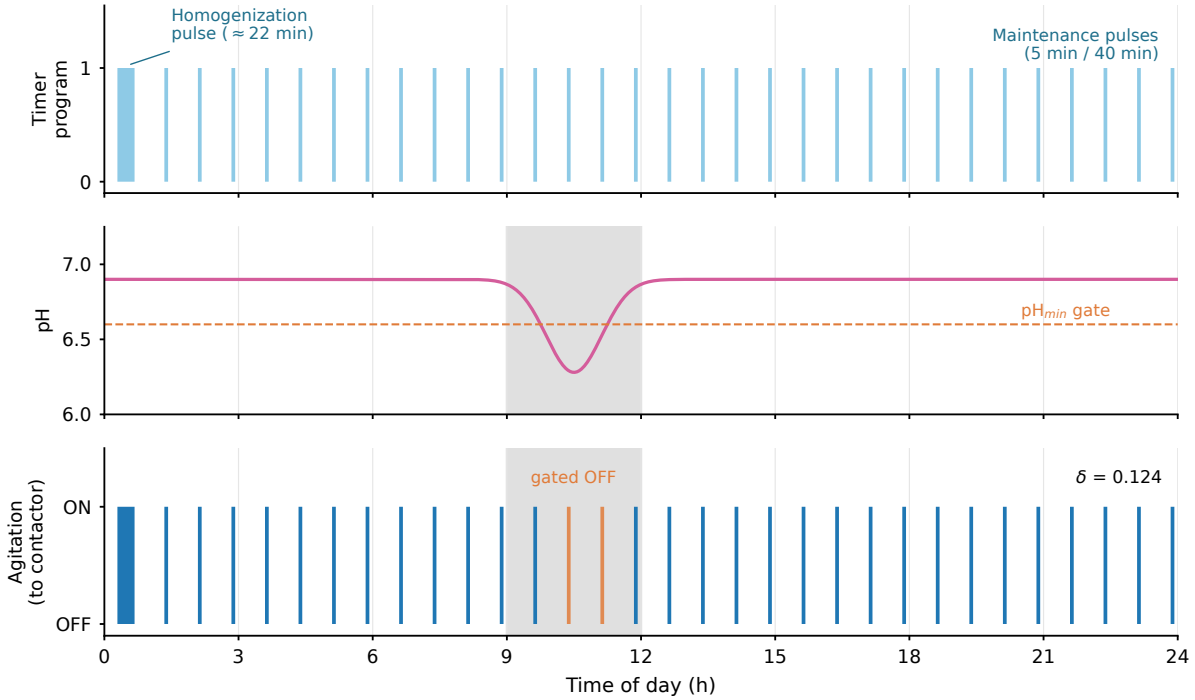

Figure 9. Substrate-driven agitation program over 24 h for the case study: After the feeding event, the homogenization pulse is executed; short maintenance pulses (5 min every 40 min) sustain substrate–biomass contact; and the pH gate inhibits agitation during a simulated acidification window ($\delta = 0.124$).

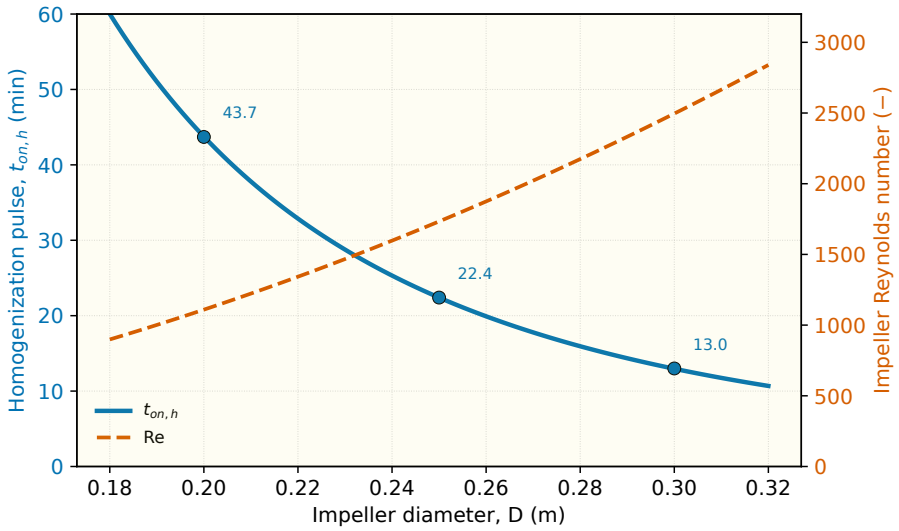

Figure 10. Sensitivity of the homogenization pulse $t_{on,h}$ and impeller Reynolds number to the impeller diameter. The strong dependence $t_{on,h} \propto D^{-3}$ makes confirmation of D from the manufacturing drawings critical for the timing setpoint.

3.7. Selected Control Variables and Supervisory Architecture

Application of the influence×feasibility criterion (Section 2.10) yields the hierarchy shown in Figure 11. Under a stability-centered weighting, the viable control set consists of

pH ($S = 4.6$), electrical conductivity ($S = 4.4$), temperature ($S = 4.3$), and level ($S = 3.9$). These four variables combine high process sensitivity or actuation relevance with low-cost, robust, consumable-free sensors, making them suitable for rural environments. In contrast, higher-complexity variables—ORP ($S = 3.3$), biogas flow/pressure ($S = 3.1$), alkalinity by titration ($S = 2.6$), and volatile fatty acids via titration/chromatography ($S = 2.5$)—fall below the threshold: although some are inherently informative, their cost, consumable requirements, or calibration fragility make them unsuitable as primary control variables in rural digesters. This result is consistent with the pH- and EC-based control framework previously formalized by the authors [34], and extends it to agitation governance.

Oxidation–reduction potential deserves a separate remark. Its sensor cost is not a limitation—combined pH/ORP electrodes sharing a single transmitter are inexpensive, and the criterion is scored accordingly—and its composite score ($S = 3.3$) is the highest among the excluded variables. It nevertheless remains below the viability threshold for two reasons independent of cost. First, in a sulfide-rich anaerobic medium the measured potential is a mixed potential rather than a thermodynamically defined redox state: the platinum surface is progressively poisoned by sulfides, the response is slow and drift-prone, and the reading is strongly pH-dependent, so ORP contributes limited information independent of the pH channel already used by the gate. Second, its demonstrated control application in anaerobic digestion is the regulation of micro-aeration for hydrogen sulfide abatement and for volatile fatty acid control, for which validated setpoints exist [50,51], whereas no equivalent threshold has been established for enabling or inhibiting agitation. ORP is therefore identified as the primary candidate for a future extension of the control set, and not as a variable excluded on cost grounds.

The resulting control architecture (Figure 4) couples the substrate-driven feedforward schedule with a feedback supervisory layer based on the four selected variables: temperature rescales the duration of the homogenization pulse, while pH, EC, and level act as logical gates that enable or inhibit the agitation signal to the actuator. In this way, agitation never operates under conditions that compromise stability (acidification or dry running), and methane production is improved as a consequence of maintaining the process within its stability window, rather than by targeting it as a direct control objective.

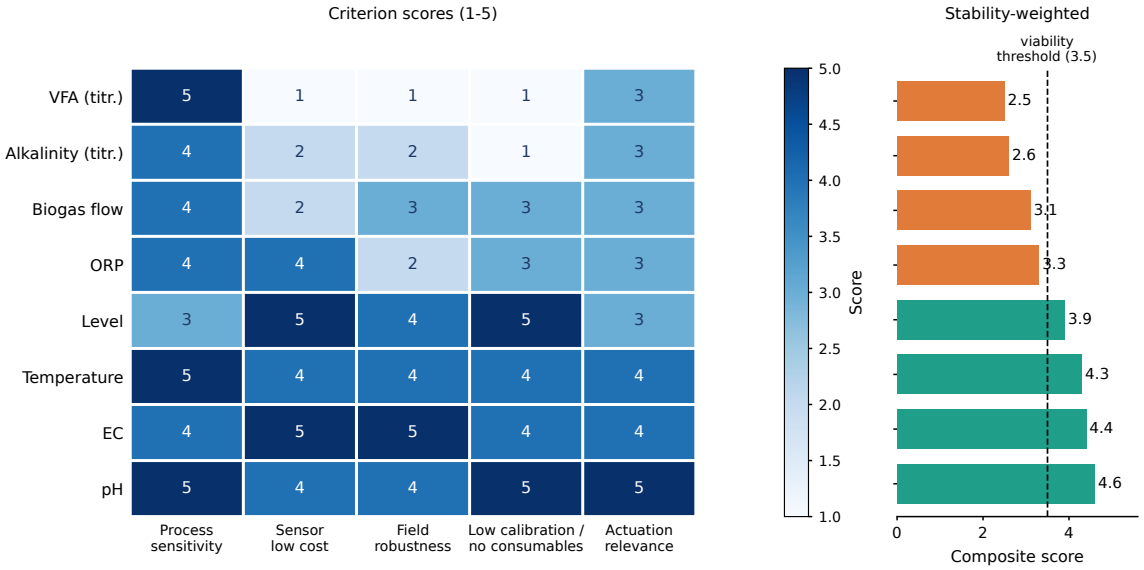

Figure 11. Influence × feasibility decision matrix for control variable selection (1–5 scoring scale per criterion; right bar: weighted composite score, $w = (0.30, 0.20, 0.20, 0.15, 0.15)$). The feasible set (pH, EC, temperature, level) dominates over high-cost or low-field-robustness variables; ORP ranks highest among the excluded variables.

3.8. Closed-Loop Dynamic Behavior Under Perturbations

The dynamic model (Section 2.11) demonstrates the controller response to an acid shock, with an agitation optimum that emerges from the physics of the contact–shear coupling rather than from parameter tuning (Figure 12 and 13). In steady state, all three modes deliver approximately 3.42 $m^3\,CH_4\,d^{-1}$ ($\eta_{bio} \approx 0.21$, consistent with the observed production).

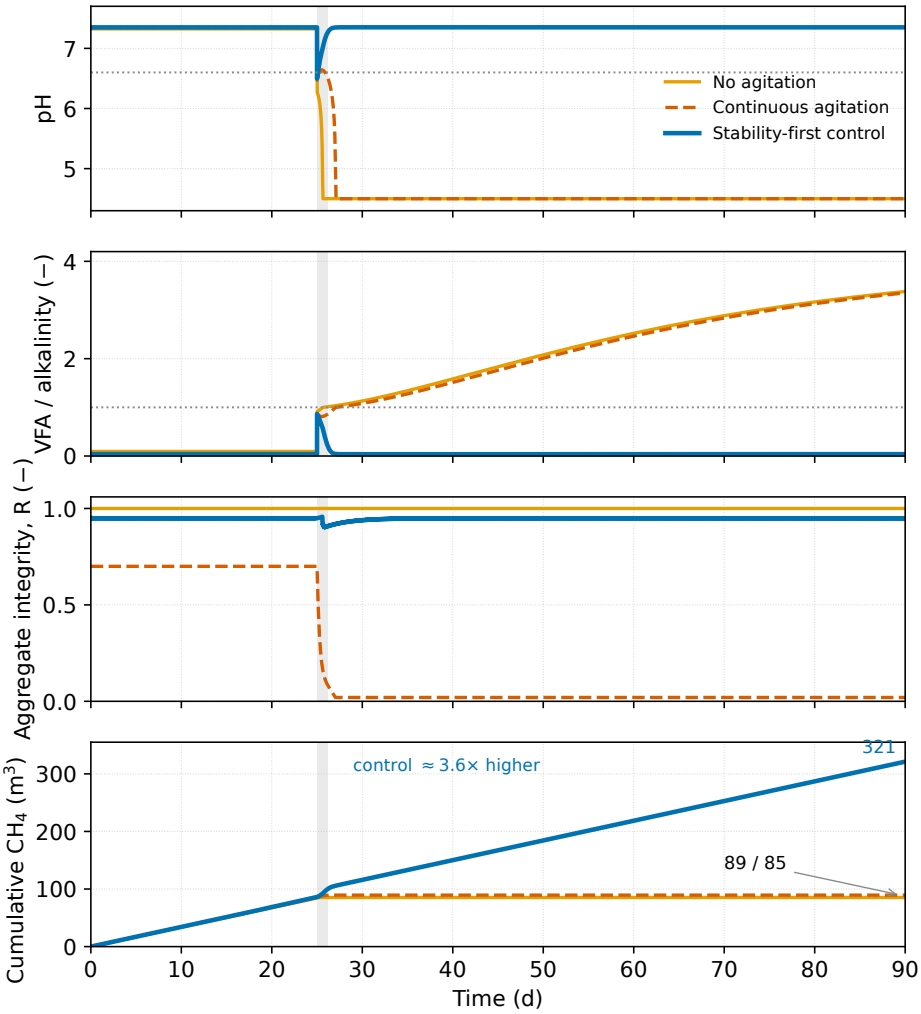

Figure 12. Closed-loop dynamic simulation (90 d) under an acid shock (shaded band, day 25): pH, VFA/alkalinity ratio, methanogenic aggregate integrity R, and cumulative methane production for the three modes. Continuous agitation destroys aggregates via shear ($R \to 0$); the no-agitation mode preserves R but fails due to contact deficit; only the stability-first controller restores process performance.

The coincidence at baseline is not due to a small contact penalty—the no-agitation mode reaches $\eta_c = 0.40$, a factor of 1.9 below the controlled mode—but to the fact that the reactor is hydrolysis-limited under nominal loading. At steady state $X_s = D_h S_{in}/(D_h + k_{hyd} f_T) = 7.7\ g\,COD\,L^{-1}$ and $r_{hyd} = r_m = 0.98\ g\,COD\,L^{-1}\,d^{-1}$ irrespective of η_c and R, because the volatile fatty acid pool S_a self-adjusts to close the balance; methanogenesis retains spare capacity and mixing cannot raise baseline throughput.

This has a methodological consequence that must be stated plainly. The dynamic model is a testbed for stability under perturbation, not a predictor of yield, and it neither reproduces nor supports the improvement in η_{bio} discussed in Section 3.4. That improvement is expected from a different mechanism—the elimination of dead zones and of the

surface crust, that is, an increase in the effectively active volume—which a perfectly mixed lumped model cannot represent by construction, and whose quantification requires the tracer or CFD verification identified as future work. The two mechanisms are therefore complementary and are kept separate throughout: contact governs stability, active volume governs yield.

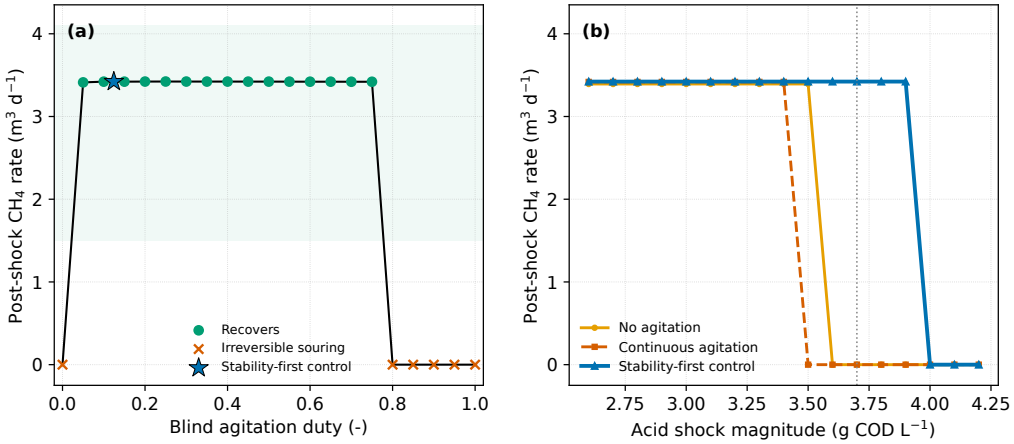

Figure 13. Emergent agitation optimum. (**a**) Duty-cycle sweep under a blind policy: A survival band bounded by collapse due to contact deficit (left) and shear (right); the star marks the stability-first controller. (**b**) Shock tolerance envelope: Post-shock methane production rate versus acid spill severity for the three modes; the controller tolerates approximately 14% higher shock severity than continuous agitation, and a region exists where only the controller survives (reference line: 3.7 g COD L^{-1} shock).

The decisive divergence emerges after the acid shock (3.7 g COD L^{-1} spill on day 25), revealing two physically distinct failure mechanisms.

Under **continuous agitation**, sustained shear stress applied to acid-weakened aggregates leads to their disintegration: structural integrity collapses ($R \to 0.02$), methanogenesis ceases, volatile fatty acids rise to a VFA/alkalinity ratio of approximately 3.4, and the process undergoes irreversible acidification (post-shock production is null; Figure 12). Under the **no-agitation mode**, in contrast, aggregates remain intact ($R = 1.00$)—no shear is applied—but the loss of feed homogenization ($\eta_c \to 0.40$) prevents the system from dissipating the shock before hydrolysate accumulation blocks the reactor, leading again to irreversible failure. In other words, the two extremes fail due to opposite mechanisms: one through mechanical destruction of biomass, the other through a contact deficit. Only the **SD-PLC control** survives: the pH gate automatically inhibits agitation during the acidification window (Figure 14, duty cycle drops to zero), preserving aggregates ($R \geq 0.90$) while maintaining sufficient mixing to recover methanogenesis to its baseline value (3.42 $m^3\,d^{-1}$). Over a 90-day cumulative horizon (starting from steady state), the controller produces 321 m^3 of CH_4 compared with 89 m^3 (continuous agitation) and 85 m^3 (no agitation), a factor of approximately 3.6.

Figure 13 generalizes this finding. The sweep of duty cycle under a *blind policy* (Figure 13a) reveals a survival band bounded by collapse at both extremes: below $\delta \approx 0.05$ the reactor fails due to contact deficit, and above $\delta \approx 0.75$ it fails due to shear; the agitation optimum is therefore not a numerical artifact but the consequence of two opposing physical costs. The reconciled program of Section 3.6 ($\delta = 0.124$) lies inside this band with a factor of 2.5 of margin against the lower boundary, which is the quantitative reason for adopting the contact criterion of Equation (15) rather than a longer maintenance interval. The stability-first controller operates within this band and, more importantly, *without relying on a fixed optimal value*, since it schedules agitation based on acid-state conditions rather than time averaging. The tolerance envelope (Figure 13b) quantifies the margin: the

shock thresholds leading to irreversible acidification are 3.5 g COD L^{-1} (continuous), 3.6 (no agitation), and 4.0 (control). The controller thus expands the recoverable operating envelope by approximately 14% relative to continuous agitation, and there exists a severity window (3.6–3.9 g COD L^{-1}) in which only the stability-first strategy preserves the process.

This result explicitly reconciles the model behavior with Stage 3 of the methodology: the absence of gravitational stratification (which relaxes the *maintenance mixing* requirement on sedimentation grounds) coexists with a real demand for *homogenization* of non-gravitational origin, which is precisely what the contact criterion quantifies. It further confirms the central thesis through a closed-loop mechanism: continuous agitation is the dangerous strategy under perturbation, while the stability-first controller preserves the process—and consequently production—by modulating mixing according to acid–base state. It must be stated transparently that the quantitative results are illustrative and anchored, not fully calibrated; the collapse of continuous agitation due to shear is a robust and mechanistically supported result [48,49], whereas the exact position of the tolerance envelope boundaries and the low-contact failure limit depends on model parameters and reactor loading margin. Full closure of these values requires rheological measurement (τ_0) and field validation, identified as future work.

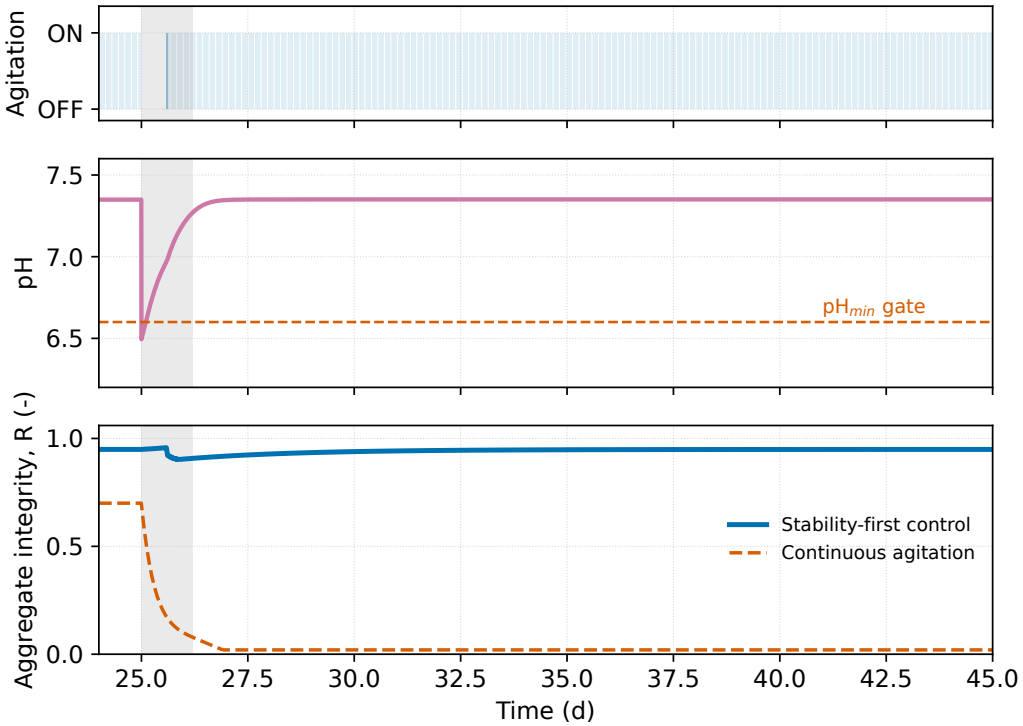

Figure 14. pH gate action during the shock (detail): The controller inhibits agitation while pH remains below threshold, preserving methanogenic aggregate integrity ($R \geq 0.90$) compared to the collapse ($R \to 0.02$) observed under continuous agitation. This is the operational realization of the stability-first logic.

4. Discussion

The contribution of this work must be positioned precisely with respect to three strands of the literature. First, mechanical agitation in fixed-dome digesters is not new, and PLC/SCADA automation with intermittent mixing timers is established industrial practice [15,16]; what these implementations do not provide is a derivation of timing setpoints from the substrate. The SD-PLC methodology is that derivation, and constitutes the claimed novelty. Second, co-digestion of guinea pig manure has been studied, including in Andean and Peruvian contexts [27,31]. Third, previous work by the authors on the

same reactor addressed geometric and operational improvements [7] and pH/EC reactive control [34]; none of these proposed a control design procedure. The present work differs in its object: a reproducible mapping from characterization to control law, in which pH/EC act here as a biological gate rather than as primary controlled variables.

4.1. Positioning with Respect to Anaerobic Digester Control

To establish the novelty of the methodology relative to the state of the art in digester automation, Table 9 contrasts representative works in AD control and automation with the SD-PLC proposal across four axes: control platform and strategy, variables actually controlled, basis for timing setpoints, and—the discriminating axis—whether mixing timing is derived from substrate characterization.

Table 9. Positioning of the SD-PLC methodology with respect to representative works on control and automation of anaerobic digestion. The discriminating axis is the last column: in no prior work is mixing timing derived from measured substrate properties.

Study	Platform/Strategy	Controlled Variables	Basis for Timing Setpoints	Mixing Timing Derived from Substrate?
Bernard et al. [52]	Software sensors + adaptive control	VFA, alkalinity, flow rate	Dynamic model/observers	No
Nguyen et al. [25] (review)	Overview of automatic control	OLR, pH, alkalinity, biogas	Various (feedback/model-based)	No: mixing is rarely a control variable
Ahmed & Rodríguez [53]	Model predictive control (MPC)	Feeding/start-up load	Predictive model	No (controls feeding)
Lara-Cisneros et al. [54]	Extremum-seeking control	Methane production	Online dynamic optimization	No
Ghanavati et al. [55]	Adaptive MPC + fuzzy supervisor	Feeding, VFA	Model + fuzzy logic	No
Alcaraz-González et al. [56]	Robust multivariable regulation	Alkalinity states	Model/experimental validation	No
Scarcello et al. [57]	Three-unit PLC architecture	Temperature, pH (range)	Generic optimal range	No
Industrial PLC/SCADA implementations	On–off PLC/SCADA	Level, temperature, pressure, agitator	Empirical/default timers	No: mixing timers are empirically fixed
SD-PLC (this work)	PLC ladder + supervisory layer	pH, EC, T, level (gating) + actuated mixing	Rheology + contact + net energy + acid–base dynamics	Yes: homogenization pulse, maintenance pulses, δ^*, and gating logic

The reading of Table 9 delimits the contribution. As synthesized in reviews of instrumentation and process control [24–26], automatic control of AD has matured along two directions: model-driven advanced control [52–56,58], increasingly assisted by soft sensors and machine learning [59–61] and acting on feeding to stabilize volatile fatty acids; and industrial PLC/SCADA automation [57], which maintains temperature, pH, level and pressure within set ranges. The critical review by Nguyen et al. [25] confirms this panorama and, revealingly for our argument, notes that mixing rarely appears as a controlled variable and that, when automated, its timing is typically set empirically. None of these lines derives mixing timing—how long to homogenize after feeding, how frequently to resuspend, and when to inhibit agitation—from measured substrate properties; it is precisely this missing link that the SD-PLC methodology formalizes. The distinction is not semantic: the predictive control of Ahmed and Rodríguez [53] is superior to ours for

governing feeding, but does not answer when and how much to agitate. SD-PLC is a feedforward scheme with a gating layer, not an optimal closed-loop controller, chosen for its low cost and feasibility in a modest rural PLC; its value lies in the origin of its setpoints, not in algorithmic sophistication. The dynamic model (Section 2.11) provides the mechanistic justification for why that origin matters: since optimal agitation depends on the acid–base state—continuous mixing fails due to shear, while no mixing fails due to contact deficit—an empirically fixed schedule can only by chance fall within the narrow safe operating window that is explicitly identified by a substrate-derived policy.

Against dominant strategies for Chinese fixed-dome digesters, the reformulation is clear. Jegede et al. [8,9] improved mixing via a self-agitating baffle that exploits biogas pressure variation, reducing dead zones; CFD studies of fixed-dome systems further show that optimizing mixing frequency breaks surface crusts and increases methane yield [11]. These approaches are effective but share a limitation: mixing intensity and timing are not independent control variables—they are dictated by geometry and gas dynamics—and therefore cannot be adjusted during operation according to substrate conditions or energy constraints. The present work converts mixing into an actuated and programmable degree of freedom, subordinated to a net energy constraint. This reformulation is supported by mixing literature converging on two points: intermittent mixing matches or outperforms continuous mixing in biogas yield while reducing energy demand [14–16,18,19,62], and mixing electricity consumption can account for roughly one third to one half of total plant demand [17]. For a small plant generating $\sim$10 kWh d^{-1}, these facts directly determine feasibility. The dynamic representation adds an independent mechanistic argument: under acid shock, continuous agitation is not only energetically wasteful but actively harmful, since shear disrupts methanogenic aggregates and triggers irreversible acidification [48,49], whereas the opposite mode—no agitation—fails due to contact deficit. The intermediate optimum governed by the acid–base state thus emerges from the competition between two physical costs rather than from a design preference.

The rheological analysis clarifies why agitation is required and how much. The co-digestion sludge is pseudoplastic, with an apparent viscosity that places the impeller in the transitional regime ($Re \approx 0.9$–2.6×10^3), rather than the turbulent regime assumed by the naive application of $P = N_p \rho N^3 D^5$. Cattle, pig and dairy manure rheology is well documented as pseudoplastic with yield stress [20,21]; guinea pig manure is not, which constitutes a primary data gap and the input that completes the methodology.

The characterization also reframes the objective quantitatively. The Buswell–Boyle potential of the 30:70 mixture (371 mL CH_4 g^{-1} VS) sets an upper bound against which the observed field conversion ($\eta_{bio} \approx 0.21$) reaches only about one-fifth. This gap is consistent with Peruvian low-temperature digestion evidence, where internal temperatures of 16–25 °C limit conversion even under long hydraulic retention times [27–30]. Improving homogenization and eliminating dead zones and surface crusts are well-established levers for increasing BDI in fixed-dome digesters [11,16], and balanced co-digestion is a complementary pathway for increasing yield and mitigating GHG emissions widely supported in manure digestion studies [4,5,63]. A substantive nuance emerging from our own stoichiometric calculations is that the mixture C/N ratio (19.2) lies below the commonly cited optimum range (20–30), consistent with low C/N manures [4]; and that adding organic residues, while useful for waste management and dilution, does not necessarily maximize performance and may increase ammonia nitrogen, a well-known inhibitory factor in manure-based AD [3]. This reinforces that the 30:70 mixture should be justified on waste management and dilution grounds, rather than on biogas yield maximization.

A direct consequence of applying the method to this particular feedstock is that the blend itself is identified as a redesign lever. Because the organic-waste fraction lowers

both the volatile matter content and the C/N ratio of the mixture (Table 4), the 30:70 blend is justified on waste-management and dilution grounds and not on yield grounds—a distinction the method makes explicit rather than conceals. A stoichiometric balance on the elemental analysis of Table 3 indicates that, starting from guinea pig manure (C/N = 20.1), a co-substrate with C/N $\gtrsim$ 55 contributing approximately 30% of the volatile solids would move the mixture into the commonly cited 20–30 optimum. Andean lignocellulosic residues such as maize stover and barley straw fall in that range, are locally available in the Chillón Valley, and their co-digestion with guinea pig manure has already been demonstrated [31].

Replacing the organic waste with such a co-substrate would, however, remove the dilution service it currently provides ($W = 87.9\%$), increasing the external water demand and—through the resulting rise in total solids and yield stress—lengthening the homogenization pulse and raising the mixing energy. This trade-off is precisely the coupling that the SD-PLC framework renders visible: the blend cannot be optimized on biochemical grounds alone, because it simultaneously fixes the rheology that governs the parasitic energy demand. Its quantitative resolution requires the rheological characterization identified as pending and is proposed as the natural continuation of this work.

4.2. Failure Modes Beyond the Reach of the Controller

A distinct and more severe scenario than a transient acid shock is the irreversible loss of one of the microbial populations, typically the acetoclastic methanogens. The controller cannot reverse such an event: once the methanogenic population has been washed out or destroyed, no mixing policy restores it, and recovery requires suspension of feeding and reinoculation—actions belonging to a supervisory layer above the mixing logic. What the controller does is reduce the probability of reaching that state, by preventing shear from being applied to acid-weakened aggregates ($R \geq 0.90$ against $R \to 0.02$ under continuous agitation, Figure 14) and by bounding the cumulative shear dose through the duty-cycle ceiling, which widens the shock tolerance envelope by approximately 14% (Figure 13b). In addition, the ladder program was extended with a collapse latch: if the gate condition $\mathrm{pH} < \mathrm{pH}_{min}$ persists for longer than a configurable interval t_{col} (72 h by default), the PLC latches a failure alarm, inhibits the inlet motor and requires manual reset, so that an unrecoverable biological event results in a safe stop and an operator notification rather than in the continued loading of a dead reactor. The latch does not attempt to diagnose which population has been lost; it only prevents the automation from masking the failure.

The supervisory layer is, by design, indirect: it acts on the acid–base state and treats methane throughput as a consequence. This leaves the controller blind to internal perturbations whose signature in pH and electrical conductivity is slow or ambiguous—a selective inhibition, or a progressive washout of methanogenic biomass—even though gas production responds immediately. A qualitative gas-production indicator is therefore incorporated as a diagnostic input rather than as a control variable. In a fixed-dome digester this measurement is almost free: gas storage is intrinsically coupled to dome pressure and to the displacement of slurry into the compensation chamber, so a low-cost pressure transducer—or a differential level reading in the compensation chamber, which is already instrumented—yields a qualitative flag (gas production normal, degraded or absent) without adding a flowmeter; low-cost IoT monitoring platforms for small-scale digesters have demonstrated the feasibility of this class of instrumentation in rural settings [64]. The distinction between control variables, which gate the actuator, and diagnostic variables, which raise alarms only, resolves the apparent tension with the ranking of Figure 11, where biogas flow falls below the threshold as a control variable while remaining valuable as a watchdog.

The estimation of methane production through a soft sensor is retained as future work. Soft sensors and machine-learning estimators for anaerobic digestion are well established [59–61], but their deployment requires a calibration dataset that this installation does not yet possess and which the field validation campaign of Stage 8 is intended to generate. Proposing a soft sensor without such a dataset would reproduce, in a different form, the very problem this work sets out to solve: a control element whose parameters are not traceable to a measurement.

4.3. Indicative Cost of the Automation System

Three remarks frame these figures. First, the mechanical mixing train—two gearmotors, shafts and marine propellers—is already installed, so the values above represent the incremental cost of converting an existing agitation system into a substrate-driven controlled one, not the cost of the plant. Second, the operating cost is small: at the reconciled duty cycle the parasitic demand is ≈2.6 kWh d^{-1} (≈960 kWh yr^{-1}, of the order of 190 USD yr^{-1} at 0.20 USD kWh^{-1}), against a gross electrical potential of 10.3 kWh d^{-1} at the present realization factor. Third, the benefit is dominated by the projected improvement in η_{bio}: raising it from 0.21 to the 0.35–0.50 band adds 2.4–4.9 m^3 CH_4 d^{-1} which, valued as substitution of liquefied petroleum gas (1 m^3 CH_4 ≈ 10 kWh ≈ 0.78 kg LPG at 1.3–1.5 USD kg^{-1}), corresponds to 880–2100 USD yr^{-1}, giving a simple payback of roughly one to four years. These are design-level estimates and must be read as an order of magnitude: the improvement in η_{bio} is a target derived from the theoretical–realized gap and from the mixing literature, not a measured outcome of this installation, and the payback interval is conditional on the field validation campaign.

To assess the practical feasibility of implementing the proposed SD-PLC automation, an indicative estimate of the required capital cost was prepared using 2026 Peruvian market ranges for the main instrumentation, control, electrical, and engineering components. The resulting cost breakdown is summarized in Table 10.

Table 10. Indicative capital cost of the SD-PLC automation system (Peruvian market, 2026).

Item	Range (USD)
Compact PLC (≥8 DI/6 DO, one analog module) and 24 VDC supply with backup	250–450
Industrial pH electrode and transmitter (immersion, digestate-rated)	200–450
Electrical conductivity sensor and transmitter	150–350
Temperature sensor (Pt100) and transmitter	40–90
Level transducers ×2 (reactor and inlet chamber)	160–400
Dome pressure transducer (diagnostic)	60–150
IP65 enclosure, contactors, motor protection, wiring and terminals	250–450
Engineering, programming and commissioning	200–400
Total, excluding HMI	1310–2740
Optional HMI panel	150–350

4.4. Limitations

Several limitations constrain these conclusions and define future work. Rheology is characterized using density and representative apparent viscosity intervals rather than a full flow curve; measuring K, n, and τ_0 for the actual mixture would close the Metzner–Otto

estimation and establish whether the gravitational or the contact criterion governs the maintenance interval. Observed performance and η_{bio} are strongly temperature-dependent, which is not actively controlled in this ambient reactor; at the low mesophilic temperatures of the Chillón Valley, a 30-day HRT may lie near the lower feasibility limit, and temperature—together with mixing—governs the gap with respect to the theoretical potential. The temperature rescaling of Equation (18) is likewise specified but not instantiated, since E_μ and m have not been determined for this slurry. The reported $\eta_{bio} \approx 0.21$ is a design-anchored estimate; a BMP experimental assay of the actual mixture would replace it with a measured BDI. The dynamic model is illustrative rather than fully calibrated: it reproduces the qualitative structure of controller behavior—shear-induced collapse under continuous agitation and protection under gating—but the exact location of the tolerance envelope boundaries depends on parameters requiring experimental identification, and, as established in Section 3.8, it does not model the active-volume mechanism on which the projected gain in η_{bio} depends. Its scope is further limited to transient acid shock conditions; sustained organic overloading is primarily a feeding-control problem that lies outside the mixing-only logic. Finally, the net energy balance is a design-level estimate; field validation using measured methane yield, motor power during agitation pulses (to determine f_L and P_{mix}), and verification of mixed volume via tracer tests or CFD [13] constitutes the natural next step. These limitations do not weaken the central contribution—a reproducible substrate-driven control design methodology—but they do bound the confidence of the quantitative estimates.

5. Conclusions

This work proposed and demonstrated a Substrate-Driven PLC Control (SD-PLC) design methodology for fixed-dome biodigesters. Its contribution is a single transferable principle: every mixing timing setpoint—homogenization pulse, maintenance interval, duty-cycle ceiling and biological gate—is derived from a measured substrate property, an explicit energy constraint or an acid–base criterion, and none of them from a default timer.

Three quantitative outcomes bound the method for the Chillón case study. The apparent viscosity of the co-digestion slurry places the impeller in the transitional regime ($Re \approx 0.9$–2.6×10^3 at the dilution actually fed), which invalidates the turbulent power correlation commonly applied in digester design and shows that installed power is governed by start-up torque and resuspension. The derived homogenization pulse is ≈22 min, with a third-order geometric sensitivity (13–44 min for $D = 0.30$–0.20 m) that makes confirmation of the impeller diameter a design-critical measurement rather than a detail. The maintenance interval is closed by a substrate–biomass contact criterion at $t_{off,m} \leq 42$ min, giving a reconciled duty cycle $\delta \approx 0.13$ that lies a factor of four below the net-energy ceiling ($\delta^* \approx 0.56$); the binding constraint is therefore physical, not energetic.

The closed-loop analysis established why the origin of the setpoints matters. Continuous agitation fails by shear-induced disintegration of acid-weakened methanogenic aggregates; the absence of agitation fails by contact deficit; only the stability-first policy survives the acid shock, with a cumulative methane production approximately 3.6 times higher over 90 days. The agitation optimum is a physical consequence of two competing costs rather than a tuned parameter, and an empirically fixed schedule can fall inside the safe window only by chance.

Two measurements close the method: the yield stress of guinea pig manure slurry—currently absent from the literature—which determines whether the gravitational or the contact criterion governs the maintenance interval, and field validation of the timing program through tracer tests, gas response and motor power monitoring. Within these

bounds, SD-PLC converts mixing in fixed-dome digesters from an operational habit into a designed, substrate-derived and energy-constrained degree of freedom.

Author Contributions: Conceptualization, Y.C.A., R.J.B., R.Á.C.J. and R.P.M.; methodology, Y.C.A., R.J.B., R.Á.C.J. and R.P.M.; software, A.S.W.F.D., D.G.B.C., C.D.P.V. and R.Á.C.J.; validation, Y.C.A., R.J.B., F.M.C.L., R.Á.C.J. and R.P.M.; formal analysis, Y.C.A., R.J.B., R.Á.C.J. and R.P.M.; investigation, Y.C.A., A.S.W.F.D., D.G.B.C., R.J.B., C.D.P.V., F.M.C.L., R.Á.C.J. and R.P.M.; resources, Y.C.A., A.S.W.F.D., D.G.B.C., C.D.P.V., F.M.C.L. and R.P.M.; data curation, A.S.W.F.D., D.G.B.C., C.D.P.V. and F.M.C.L.; writing—original draft preparation, Y.C.A., R.J.B., R.Á.C.J. and R.P.M.; writing—review and editing, Y.C.A., A.S.W.F.D., D.G.B.C., R.J.B., C.D.P.V., F.M.C.L., R.Á.C.J. and R.P.M.; visualization, A.S.W.F.D., D.G.B.C., C.D.P.V. and F.M.C.L.; supervision, Y.C.A., R.J.B., R.Á.C.J. and R.P.M.; project administration, Y.C.A., R.J.B., R.Á.C.J. and R.P.M. All authors have read and agreed to the published version of the manuscript.

Funding: This research was funded by the Universidad Tecnológica del Perú under project P-2024-LIM-20 "Improving biogas production efficiency through optimized design of Chinese-type biodigesters: case study of a 20 m^3 digester in the Chillón Valley".

Institutional Review Board Statement: Not applicable.

Data Availability Statement: Data supporting the results are available from the corresponding author upon reasonable request.

Acknowledgments: Special thanks are extended to the Universidad Tecnológica del Perú and the Asociación de Productores Ecológicos del Valle Chillón.

Conflicts of Interest: The authors declare no conflict of interest.

Nomenclature and Abbreviations

Latin symbols

A_{ch}	Inlet-chamber cross-sectional area	m^2
A_b, A_T	Residual bicarbonate and total alkalinity	meq L^{-1}
BMP_{th}	Theoretical biochemical methane potential	mL CH_4 g^{-1} VS
D	Impeller diameter	m
D_h	Dilution rate, 1/HRT	d^{-1}
d_{crit}, d_p	Critical suspension and particle diameter	m
E_{el}, E_{th}	Recoverable electrical and available thermal energy	kWh d^{-1}
E_{net}, E_{par}	Net balance and parasitic mixing demand	kWh d^{-1}
E_μ	Viscous activation energy	J mol^{-1}
F_{col}	Collapse latch flag	–
f_L, f_{reg}, f_{sv}	Load, regime-penalty and overdesign factors	–
f_{prog}	Binary output of the feedforward timing program	–
G	Camp velocity gradient	s^{-1}
H, L	Usable and measured liquid height	m
I_{pH}, I^h_{pH}	pH inhibition functions	–
K, n	Consistency index and flow behaviour index	Pa s^n, –
K_S	Half-saturation constant for acetate uptake	g COD L^{-1}
k_{MO}	Metzner–Otto constant	–
k_{hyd}, k_m, k_d	Hydrolysis, methanogenesis and decay constants	d^{-1}
k_{mix}, k_{seg}	Homogenization and segregation constants	d^{-1}
k_{sh}, k_{rec}	Shear disintegration and aggregate recovery constants	d^{-1}
M, M_w	Daily feed mass and dilution water	kg d^{-1}
N	Impeller rotational speed	rev s^{-1}
N_p, N_Q	Power number and pumping number	–
n_c	Number of tank turnovers	–
P, P_{mix}	Impeller shaft power and installed mixing power	W, kW

p_{dome}	Dome gauge pressure	mbar
Q, Q_{in}	Daily and instantaneous feed flow	$m^3\,d^{-1}$
Q_{CH_4}	Methane production rate	$m^3\,d^{-1}$
R	Methanogenic aggregate integrity, $R \in [0,1]$	–
R_g	Universal gas constant	$J\,mol^{-1}\,K^{-1}$
Re	Impeller Reynolds number	–
r_{hyd}, r_m	Hydrolysis and methanogenesis rates	$g\,COD\,L^{-1}\,d^{-1}$
S_a	Volatile fatty acids expressed as COD	$g\,COD\,L^{-1}$
S_{in}	Influent biodegradable COD	$g\,COD\,L^{-1}$
$S(v)$, w_k	Composite score and criterion weight	–
T, T_0	Operating and reference temperature	°C (K in Equation (18))
t_{circ}, t_{col}	Circulation time and collapse-latch threshold	s, h
$t_{on,h}$	Homogenization pulse duration	min
$t_{on,m}$, $t_{off,m}$	Maintenance pulse duration and OFF interval	min
t_{strat}, t_{cont}	Stratification- and contact-limited OFF intervals	min
u_{ag}	Agitation command signal, $u_{ag} \in \{0,1\}$	–
V, V_L	Constructed volume and mixed liquid working volume	m^3
V_d, V_{cd}	Required digestion and construction volume	m^3
v_s, v_{tip}	Hindered settling velocity and impeller tip speed	$m\,s^{-1}$
X_s, X_m	Particulate COD and methanogenic biomass	$g\,COD\,L^{-1}$
$Y_{g,crit}$	Critical gravitational yield number	–
Y_x, Y_{CH_4}	Biomass and methane yield coefficients	–, $L\,g\,COD^{-1}$
Greek symbols		
γ, $\dot{\gamma}$	Shear amplification factor and shear rate	–, s^{-1}
$\Delta\rho$, Δ_a	Density contrast and acid shock magnitude	$kg\,m^{-3}$, $g\,COD\,L^{-1}$
δ, δ^*, δ_{min}	Duty cycle, energy ceiling and contact floor	–
δ_D	Dirac distribution (Equation (25))	d^{-1}
ε	Numerical lower bound on residual alkalinity	$meq\,L^{-1}$
η_{bio}, η_c, η_e	Realization, contact and electrical efficiencies	–
Θ, Θ_{tgt}	Segregation index and its target value	–
λ	Contact-loss coefficient	–
μ_{app}, ρ	Apparent viscosity and mixture density	Pa s, $kg\,m^{-3}$
ρ_{lo}, ρ_{hi}	Lower and upper thresholds of the Ripley ratio	–
σ	Acid stress index, $\sigma \in [0,1]$	–
τ, τ_0	Shear stress and yield stress	Pa
ϕ	Fraction of usable height for stratification	–
Abbreviations		
AD	Anaerobic digestion	
ADM1	Anaerobic Digestion Model No. 1	
AM2	Two-step anaerobic digestion model	
BDI	Biodegradability Index	
BMP	Biochemical Methane Potential	
CFD	Computational fluid dynamics	
COD	Chemical Oxygen Demand	
EC	Electrical Conductivity	
GP	Guinea pig manure	
HRT	Hydraulic Retention Time	
MPC	Model Predictive Control	
OLR	Organic Loading Rate	
ORP	Oxidation–Reduction Potential	
PLC	Programmable Logic Controller	
RO	Organic residues	
RS	Set–Reset (latch)	
SCADA	Supervisory Control and Data Acquisition	

SD-PLC	Substrate-Driven PLC Control
VFA	Volatile Fatty Acids
VM	Volatile Matter
VS	Volatile Solids

References

1. Garfí, M.; Martí-Herrero, J.; Garwood, A.; Ferrer, I. Household anaerobic digesters for biogas production in Latin America: A review. *Renew. Sustain. Energy Rev.* **2016**, *60*, 599–614. [CrossRef]
2. Ferrer-Martí, L.; Ferrer, I.; Sánchez, E.; Garfí, M. A multi-criteria decision support tool for the assessment of household biogas digester programmes in rural areas. A case study in Peru. *Renew. Sustain. Energy Rev.* **2018**, *95*, 74–83. [CrossRef]
3. Gerber, P.J.; Steinfeld, H.; Henderson, B.; Mottet, A.; Opio, C.; Dijkman, J.; Falcucci, A.; Tempio, G. *Tackling Climate Change Through Livestock: A Global Assessment of Emissions and Mitigation Opportunities*; Food and Agriculture Organization of the United Nations (FAO): Rome, Italy, 2013.
4. Ulukardesler, A.H. Anaerobic co-digestion of grass and cow manure: Kinetic and GHG calculations. *Sci. Rep.* **2023**, *13*, 6320. [CrossRef] [PubMed]
5. Karki, R.; Chuenchart, W.; Surendra, K.C.; Shrestha, S.; Raskin, L.; Sung, S.; Khanal, S.K. Anaerobic co-digestion: Current status and perspectives. *Bioresour. Technol.* **2021**, *330*, 125001. [CrossRef] [PubMed]
6. Baek, G.; Kim, D.; Kim, J.; Kim, H.; Lee, C. Treatment of cattle manure by anaerobic co-digestion with food waste and pig manure: Methane yield and synergistic effect. *Int. J. Environ. Res. Public Health* **2020**, *17*, 4737. [CrossRef] [PubMed]
7. Castillo Alvarez, Y.; Jiménez Borges, R.; Patiño Vidal, C.D.; Carhuancho Leon, F.M.; Pinares Buendia, J.S.; Samaniego Nolasco, J.A. Design improvements and best practices in small-scale biodigesters for sustainable biogas production: A case study in the Chillón Valley, Perú. *Energies* **2025**, *18*, 338. [CrossRef]
8. Jegede, A.O.; Zeeman, G.; Bruning, H. Development of an optimised Chinese dome digester enables smaller reactor volumes; pilot scale performance. *Energies* **2019**, *12*, 2213. [CrossRef]
9. Jegede, A.O.; Gualtieri, C.; Zeeman, G.; Bruning, H. Three-phase simulation of the hydraulic characteristics of an optimized Chinese dome digester using COMSOL Multiphysics. *Renew. Energy* **2020**, *157*, 530–544. [CrossRef]
10. Jegede, A.O.; Zeeman, G.; Bruning, H. A review of mixing, design and loading conditions in household anaerobic digesters. *Crit. Rev. Environ. Sci. Technol.* **2019**, *49*, 2117–2153. [CrossRef]
11. Agborambang, M.E.; Fujiwara, M.; Bhatia, P.; Kishi, M.; Sekine, M.; Salangsang, M.C.D.; Matsuyama, T.; Toda, T. Characterization of mixing by CFD simulation and optimization of mixing frequency to break scum and enhance methane yield in a Chinese dome digester. *BioEnergy Res.* **2023**, *16*, 1177–1189. [CrossRef]
12. Shrestha, S.; Lohani, S.P. CFD analysis for mixing performance of different types of household biodigesters. *Clean. Energy* **2022**, *6*, 325–334. [CrossRef]
13. Caillet, H.; Bastide, A.; Adelard, L. Advances in computational fluid dynamics modeling of anaerobic digestion process for renewable energy production: A review. *Clean. Waste Syst.* **2023**, *6*, 100124. [CrossRef]
14. Singh, B.; Szamosi, Z.; Siménfalvi, Z. State of the art on mixing in an anaerobic digester: A review. *Renew. Energy* **2019**, *141*, 922–936. [CrossRef]
15. Singh, B.; Szamosi, Z.; Siménfalvi, Z. Impact of mixing intensity and duration on biogas production in an anaerobic digester: A review. *Crit. Rev. Biotechnol.* **2020**, *40*, 508–521. [CrossRef] [PubMed]
16. Kariyama, I.D.; Zhai, X.; Wu, B. Influence of mixing on anaerobic digestion efficiency in stirred tank digesters: A review. *Water Res.* **2018**, *143*, 503–517. [CrossRef] [PubMed]
17. Lindmark, J.; Thorin, E.; Bel Fdhila, R.; Dahlquist, E. Effects of mixing on the result of anaerobic digestion: Review. *Renew. Sustain. Energy Rev.* **2014**, *40*, 1030–1047. [CrossRef]
18. Kelif Ibro, M.; Ancha, V.R.; Lemma, D.B. Biogas production optimization in the anaerobic codigestion process: A critical review on process parameters, modeling and simulation tools. *J. Chem.* **2024**, *2024*, 4599371. [CrossRef]
19. Elsayed, M.; Andres, Y.; Meky, N.; Hassan, R. Anaerobic co-digestion of sugar beet pulp and sludge: Influence of periodic intermittent stirring and mixing ratio. *Biomass Convers. Biorefin.* **2024**, *14*, 18995–19003. [CrossRef]
20. Achkari-Begdouri, A.; Goodrich, P.R. Rheological properties of Moroccan dairy cattle manure. *Bioresour. Technol.* **1992**, *40*, 149–156. [CrossRef]
21. Hreiz, R.; Adouani, N.; Fünfschilling, D.; Marchal, P.; Pons, M.-N. Rheological characterization of raw and anaerobically digested cow slurry. *Chem. Eng. Res. Des.* **2017**, *119*, 47–57. [CrossRef]
22. Metzner, A.B.; Otto, R.E. Agitation of non-Newtonian fluids. *AIChE J.* **1957**, *3*, 3–10. [CrossRef]
23. Paul, E.L.; Atiemo-Obeng, V.A.; Kresta, S.M. (Eds.) *Handbook of Industrial Mixing: Science and Practice*; Wiley-Interscience: Hoboken, NJ, USA, 2004.

24. Jimenez, J.; Latrille, E.; Harmand, J.; Robles, A.; Ferrer, J.; Gaida, D.; Wolf, C.; Mairet, F.; Bernard, O.; Alcaraz-González, V.; et al. Instrumentation and control of anaerobic digestion processes: A review and some research challenges. *Rev. Environ. Sci. Biotechnol.* **2015**, *14*, 615–648. [CrossRef]
25. Nguyen, D.; Gadhamshetty, V.; Nitayavardhana, S.; Khanal, S.K. Automatic process control in anaerobic digestion technology: A critical review. *Bioresour. Technol.* **2015**, *193*, 513–522. [CrossRef] [PubMed]
26. DelaVega-Quintero, J.C.; Nuñez-Pérez, J.; Lara-Fiallos, M.; Barba, P.; Burbano-García, J.L.; Espín-Valladares, R. Advances and challenges in anaerobic digestion for biogas production: Policy, technological and microbial perspectives. *Processes* **2025**, *13*, 3648. [CrossRef]
27. Garfí, M.; Ferrer-Martí, L.; Villegas, V.; Ferrer, I. Psychrophilic anaerobic digestion of guinea pig manure in low-cost tubular digesters at high altitude. *Bioresour. Technol.* **2011**, *102*, 6356–6359. [CrossRef] [PubMed]
28. Ferrer, I.; Garfí, M.; Uggetti, E.; Ferrer-Martí, L.; Calderon, A.; Velo, E. Biogas production in low-cost household digesters at the Peruvian Andes. *Biomass Bioenergy* **2011**, *35*, 1668–1674. [CrossRef]
29. Alvarez, R.; Villca, S.; Lidén, G. Biogas production from llama and cow manure at high altitude. *Biomass Bioenergy* **2006**, *30*, 66–75. [CrossRef]
30. Kashyap, D.R.; Dadhich, K.S.; Sharma, S.K. Biomethanation under psychrophilic conditions: A review. *Bioresour. Technol.* **2003**, *87*, 147–153. [CrossRef] [PubMed]
31. Meneses Quelal, W.O.; Velázquez-Martí, B.; Gaibor Chávez, J.; Niño Ruiz, Z.; Ferrer Gisbert, A. Evaluation of methane production from the anaerobic co-digestion of manure of guinea pig with lignocellulosic Andean residues. *Environ. Sci. Pollut. Res.* **2022**, *29*, 2227–2243. [CrossRef] [PubMed]
32. Garfí, M.; Ferrer-Martí, L.; Perez, I.; Flotats, X.; Ferrer, I. Codigestion of cow and guinea pig manure in low-cost tubular digesters at high altitude. *Ecol. Eng.* **2011**, *37*, 2066–2070. [CrossRef]
33. Meneses-Quelal, O.; Velázquez-Martí, B.; Gaibor-Chávez, J.; Niño Ruiz, Z. Effect of the co-digestion of agricultural lignocellulosic residues with manure from South American camelids. *Biofuels Bioprod. Biorefin.* **2021**, *15*, 525–544. [CrossRef]
34. Castillo Alvarez, Y.; Jiménez Borges, R.; Patiño Vidal, C.D.; Carhuancho Leon, F.M. Sustainable valorization of bovine and guinea-pig waste: Co-optimization of pH and electrical conductivity in biodigesters. *Recycling* **2025**, *10*, 190. [CrossRef]
35. Buswell, A.M.; Mueller, H.F. Mechanism of methane fermentation. *Ind. Eng. Chem.* **1952**, *44*, 550–552. [CrossRef]
36. Boyle, W.C. Energy recovery from sanitary landfills—A review. In *Microbial Energy Conversion*; Schlegel, H.G., Barnea, J., Eds.; Pergamon Press: Oxford, UK, 1977; pp. 119–138.
37. Angelidaki, I.; Sanders, W. Assessment of the anaerobic biodegradability of macropollutants. *Rev. Environ. Sci. Biotechnol.* **2004**, *3*, 117–129. [CrossRef]
38. Hernandez-Shek, M.A.; Mottelet, S.; Peultier, P.; Pauss, A.; Ribeiro, T. Rheological characteristics of an anaerobically digested rye and maize silage mixture: Impact of solid concentration and particle size on rheological properties. *Chem. Eng. Res. Des.* **2023**, *196*, 671–684. [CrossRef]
39. Hernandez-Shek, M.A.; Mottelet, S.; Peultier, P.; Pauss, A.; Ribeiro, T. Development of devices for the determination of the rheological properties of coarse biomass treated by dry anaerobic digestion. *Bioresour. Technol. Rep.* **2021**, *15*, 100686. [CrossRef]
40. Kisielewska, M.; Debowski, M.; Zielinski, M. Preparation of samples for the study of rheological parameters of digested pulps in a bioreactor of an agricultural biogas plant. *Energies* **2024**, *17*, 965. [CrossRef]
41. Wu, B. CFD simulation of mixing for high-solids anaerobic digestion. *Biotechnol. Bioeng.* **2012**, *109*, 2116–2126. [CrossRef] [PubMed]
42. Batstone, D.J.; Keller, J.; Angelidaki, I.; Kalyuzhnyi, S.V.; Pavlostathis, S.G.; Rozzi, A.; Sanders, W.T.M.; Siegrist, H.; Vavilin, V.A. The IWA Anaerobic Digestion Model No 1 (ADM1). *Water Sci. Technol.* **2002**, *45*, 65–73. [CrossRef]
43. Bernard, O.; Hadj-Sadok, Z.; Dochain, D.; Genovesi, A.; Steyer, J.-P. Dynamical model development and parameter identification for an anaerobic wastewater treatment process. *Biotechnol. Bioeng.* **2001**, *75*, 424–438. [CrossRef] [PubMed]
44. Hassam, S.; Ficara, E.; Leva, A.; Harmand, J. A generic and systematic procedure to derive a simplified model from the Anaerobic Digestion Model No. 1 (ADM1). *Biochem. Eng. J.* **2015**, *99*, 193–203. [CrossRef]
45. Hajji, A.; Louartassi, Y.; Garoum, M.; Laaroussi, N.; Rhachi, M. Modification and extension of the anaerobic model N°2 (AM2) for the simulation of anaerobic digestion of municipal solid waste. *Int. J. Renew. Energy Dev.* **2023**, *12*, 913–922. [CrossRef]
46. Veeken, A.; Kalyuzhnyi, S.; Scharff, H.; Hamelers, B. Effect of pH and VFA on hydrolysis of organic solid waste. *J. Environ. Eng.* **2000**, *126*, 1076–1081. [CrossRef]
47. Vavilin, V.A.; Angelidaki, I. Anaerobic degradation of solid material: Importance of initiation centers for methanogenesis, mixing intensity, and 2D distributed model. *Biotechnol. Bioeng.* **2005**, *89*, 113–122. [CrossRef] [PubMed]
48. Stroot, P.G.; McMahon, K.D.; Mackie, R.I.; Raskin, L. Anaerobic codigestion of municipal solid waste and biosolids under various mixing conditions—I. Digester performance. *Water Res.* **2001**, *35*, 1804–1816. [CrossRef] [PubMed]
49. McMahon, K.D.; Stroot, P.G.; Mackie, R.I.; Raskin, L. Anaerobic codigestion of municipal solid waste and biosolids under various mixing conditions—II. Microbial population dynamics. *Water Res.* **2001**, *35*, 1817–1827. [CrossRef] [PubMed]

50. Nguyen, D.; Wu, Z.; Shrestha, S.; Lee, P.-H.; Raskin, L.; Khanal, S.K. Intermittent micro-aeration: New strategy to control volatile fatty acid accumulation in high organic loading anaerobic digestion. *Water Res.* **2019**, *166*, 115080. [CrossRef] [PubMed]
51. Anon. Hydrogen sulphide management in anaerobic digestion: A critical review on input control, process regulation and post-treatment. *Bioresour. Technol.* **2022**, *346*, 126592. [CrossRef] [PubMed]
52. Bernard, O.; Polit, M.; Hadj-Sadok, Z.; Pengov, M.; Dochain, D.; Estaben, M.; Labat, P. Advanced monitoring and control of anaerobic wastewater treatment plants: Software sensors and controllers for an anaerobic digester. *Water Sci. Technol.* **2001**, *43*, 175–182. [CrossRef]
53. Ahmed, W.; Rodríguez, J. A model predictive optimal control system for the practical automatic start-up of anaerobic digesters. *Water Res.* **2020**, *174*, 115599. [CrossRef] [PubMed]
54. Lara-Cisneros, G.; Aguilar-López, R.; Femat, R. On the dynamic optimization of methane production in anaerobic digestion via extremum-seeking control approach. *Comput. Chem. Eng.* **2015**, *75*, 49–59. [CrossRef]
55. Ghanavati, M.A.; Vafa, E.; Shahrokhi, M. Control of an anaerobic bioreactor using a fuzzy supervisory controller. *J. Process Control* **2021**, *103*, 87–99. [CrossRef]
56. Alcaraz-González, V.; Fregoso-Sánchez, F.A.; González-Álvarez, V.; Steyer, J.-P. Multivariable robust regulation of alkalinities in continuous anaerobic digestion processes: Experimental validation. *Processes* **2021**, *9*, 1153. [CrossRef]
57. Scarcello, L.; Benalia, S.; Zimbalatti, G.; Fazari, A.; Bernardi, B. A smart automation system for the management and control of a medium scale digester plant. In *AIIA 2022: Biosystems Engineering Towards the Green Deal*; Lecture Notes in Civil Engineering; Springer: Cham, Switzerland, 2023; Volume 337. [CrossRef]
58. Carecci, D.; Catenacci, A.; Ficara, E.; Ferretti, G.; Leva, A. Modelling, optimisation and control of full-scale co-digestion biomethane plants. In Proceedings of the 2024 IEEE 63rd Conference on Decision and Control (CDC), Milan, Italy, 16–19 December 2024; pp. 106–112. [CrossRef]
59. Yan, P.; Gai, M.; Wang, Y.; Gao, X. Review of soft sensors in anaerobic digestion process. *Processes* **2021**, *9*, 1434. [CrossRef]
60. Ge, Y.; Tao, J.; Wang, Z.; Chen, C.; Mu, L.; Ruan, H.; Rodríguez Yon, Y.; Su, H.; Yan, B.; Chen, G. Modification of Anaerobic Digestion Model No. 1 with machine learning models towards applicable and accurate simulation of biomass anaerobic digestion. *Chem. Eng. J.* **2023**, *454*, 140369. [CrossRef]
61. Marycz, M.; Turowska, I.; Glazik, S.; Jasiński, P. Artificial intelligence in anaerobic digestion: A review of sensors, modeling approaches, and optimization strategies. *Sensors* **2025**, *25*, 6961. [CrossRef] [PubMed]
62. Singh, B.; Kovács, K.L.; Bagi, Z.; Petrik, M.; Szepesi, G.L.; Siménfalvi, Z.; Szamosi, Z. Significance of intermittent mixing in a mesophilic anaerobic digester. *Fermentation* **2022**, *8*, 518. [CrossRef]
63. Xing, B.-S.; Cao, S.; Han, Y.; Wen, J.; Zhang, K.; Wang, X.C. Stable and high-rate anaerobic co-digestion of food waste and cow manure: Optimisation of start-up conditions. *Bioresour. Technol.* **2020**, *307*, 123195. [CrossRef] [PubMed]
64. Anon. An assessment of a solar PV-powered IoT monitoring system for small-scale biogas digesters. *Discov. Internet Things* **2025**, *5*, 122 . [CrossRef]

Disclaimer/Publisher's Note: The statements, opinions and data contained in all publications are solely those of the individual author(s) and contributor(s) and not of MDPI and/or the editor(s). MDPI and/or the editor(s) disclaim responsibility for any injury to people or property resulting from any ideas, methods, instructions or products referred to in the content.